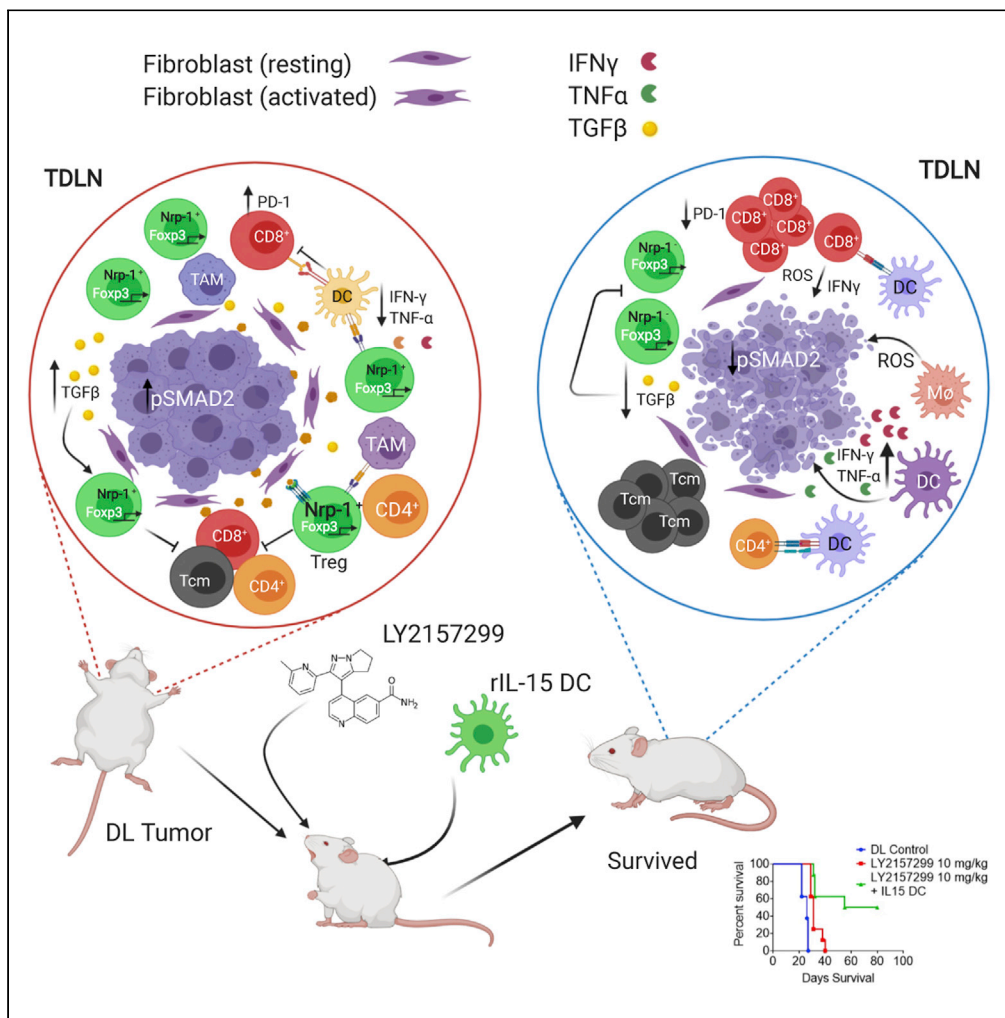Article

Galunisertib Drives Treg Fragility and Promotes Dendritic Cell-Mediated Immunity against Experimental Lymphoma

Sumit Kumar Hira, Abhinandan Rej, Ankush Paladhi, ..., Indrani Mondal, Sankar Bhattacharyya, Partha Pratim Manna

sumit.hira2008@gmail.com (S.K.H.)
pp_manna@yahoo.com (P.P.M.)

HIGHLIGHTS

Galunisertib (LY2157299) + IL-15-activated DC is tumoricidal against DL lymphoma

The binary therapy downregulates Treg cell generation in lymph nodes

Loss of p-SMAD2 and Neuropilin-1 in lymph nodes with improved prognosis

Critical role of central CD8^{+} memory T cells and Treg cells for therapeutic success

Article

Galunisertib Drives Treg Fragility and Promotes Dendritic Cell-Mediated Immunity against Experimental Lymphoma

Sumit Kumar Hira,[1,6,*] Abhinandan Rej,[1] Ankush Paladhi,[1] Ranjeet Singh,[2] Jayasree Saha,[3] Indrani Mondal,[4] Sankar Bhattacharyya,[3] and Partha Pratim Manna[2,5,*]

SUMMARY

Galunisertib (LY2157299) is a selective ATP-mimetic inhibitor of TGF-β receptor-I activation, currently under clinical trial in a variety of cancers. We have tested the combined effects of galunisertib- and interleukin-15-activated dendritic cells in an aggressive and highly metastatic murine lymphoma. Based on the tumor-draining lymph node architecture, and its histology, the combination therapy results in better prognosis, including disappearance of the disease-exacerbating regulatory T cells. Our data suggest that galunisertib significantly enhances the success of immunotherapy with IL-15-activated dendritic cells by limiting the regulatory T cells generation with consequent downregulation of regulatory T cells in the tumor-draining lymph nodes and vascularized organ like spleen. This is also associated with consistent loss p-SMAD2 and downregulation of Neuropilin-1, leading to better prognosis and positive outcome. These results connect the role of combined therapy with the consequent elimination of disease-exacerbating T regulatory cells in a metastatic murine lymphoma.

INTRODUCTION

Transforming growth factor β (TGF-β) is a critical physiological regulator of cell growth and differentiation and a key driver of cancer (Hanahan and Weinberg, 2011; Roberts et al., 1981). TGF-β has been reported to block the growth of quiescent hematopoietic stem cells and stimulate the differentiation of late progenitors to erythroid and myeloid cells (Akhurst, 2017). Loss of extracellular TGF receptors and disruption of intracellular TGF-β signaling by oncogenes is reported in various malignant and premalignant states. TGF-β also affects tumor growth and survival by influencing the secretion of other growth factors and manipulation in and around the tumor microenvironment (Bhola et al., 2013; Massagué, 2008). These changes, associated with the tumor advancement are mediated by TGF-β signaling and are also accompanied by extrinsic factors, originating from the tumor microenvironment, such as angiogenesis, inflammation, and fibroblast activation. The canonical TGF-β signaling pathway is activated by TGF-β1, TGF-β2, or TGF-β3, which binds to the TGF-β receptor II (TGF-βRII, heterodimerizes with the TGF-β-receptor I TGF-βRI or ALK5) and trans-phosphorylates the kinase domain of both receptors. This phosphorylation leads to the recruitment and phosphorylation of SMAD2 and SMAD3, which initiates SMAD signaling cascade resulting in nuclear translocation and gene transcription for a wide range of tumor-promoting mediators (Heldin et al., 1997; Heldin and Moustakas, 2012; Yang and Moses, 2008).

In many malignancies, existence of tumor cells in the tumor-draining lymph nodes (TDLN) is a key prognostic factor and sometimes predicates the course of treatment. Lymph nodes draining the primary tumor is a prerequisite for the initiation of an effective anti-tumor T cell immune response that constitutes the first line of defense against metastatic spread (Murthy et al., 2019). Here, effective priming of cytotoxic CD8^{+} T cells (T$_c$) takes place upon tumor antigen recognition, presented by dendritic cells (DCs) and macrophages. However, cancer-derived immune-repressive factors such as extracellular vesicles, IL-6, TGF-β, prostaglandin-E2 (PGE2), and vascular endothelial growth factor (VEGF) make the TDLN immune response compromised. As a result, DC maturation gets suppressed and acquires M2 macrophage-like phenotype, and will, therefore, result in improper cross-present tumor antigens in TDLN (Rotman et al., 2019). Tumor microenvironment (TME) in TDLN supports tumor growth and survival and regulates immune responses. Within the TME, the TGF-β family ligands have significant role in tumor immune evasion, leading to tumor

[1]Cellular Immunology Laboratory, Department of Zoology, The University of Burdwan, Bardhaman 713104, India

[2]Immunobiology Laboratory, Department of Zoology, Banaras Hindu University, Varanasi 221005, India

[3]Immunobiology Laboratory, Department of Zoology, Sidho Kanho Birsha University, Purulia 723104, India

[4]Department of Hematology, NRS Medical college & Hospital, 138 AJC Bose Road, Kolkata 700014, India

[5]Senior author

[6]Lead Contact

*Correspondence:
sumit.hira2008@gmail.com
(S.K.H.),
pp_manna@yahoo.com
(P.P.M.)

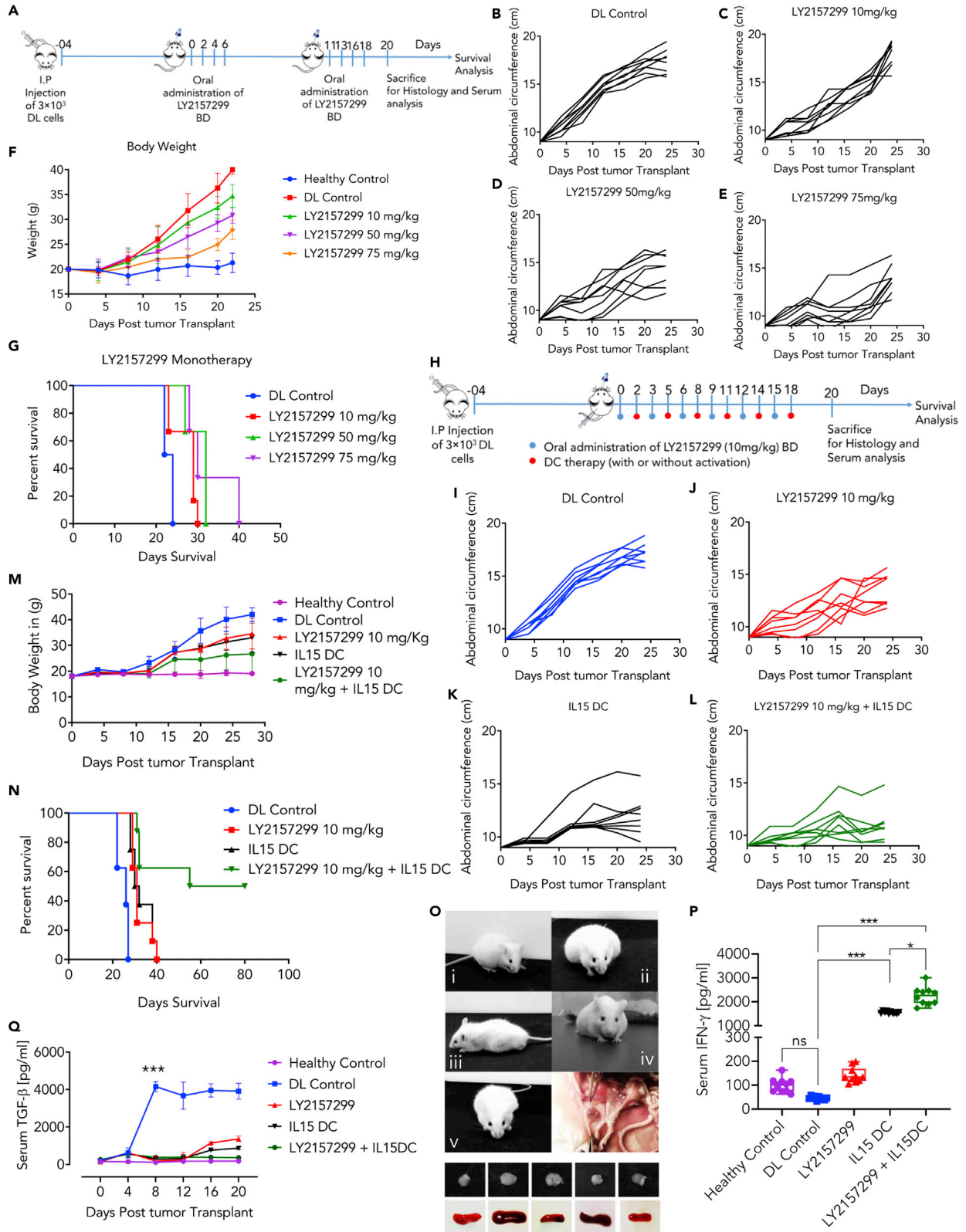https://doi.org/10.1016/j.isci.2020.101623

Figure 1. Prolonged Tumor-Free Survival and Reduced DL Tumor Development in AKR/J Mice Treated with Galunisertib + rIL15 DC Is Accompanied with Reduced Expression of TGF-β and Surge in IFN-γ

(A) Therapeutic schedule for oral administration of galunisertib.

(B–E) Measurement of abdominal circumferences (tumor volume) in mice receiving the indicated treatment. Each line represents individual animal.

(F) Body weight of the untreated and treated groups for the indicated time period. Data are presented as mean $\pm$ SD, n = 8.

(G) Kaplan-Meier survival analysis of the animals receiving the indicated treatment.

(H) Treatment schedule for galunisertib + rIL15 DC.

(I–L) The abdominal circumference (tumor volume) following indicated treatment. Each line represents single animal.

(M and N) Measurement of body weight and Kaplan-Meier survival analysis for the untreated and treated animals during the indicated time period.

(O) Photographic evidences in support of therapeutic success and corresponding splenic sizes following treatment.

(P and Q) Serum IFN-γ and TGF-β levels for the animals treated with or without galunisertib + rIL15 DC after day 22 when the untreated DL animal succumbs to death. Data presented as mean $\pm$ SD, n = 8, from summary of data of five different mice from each group.

Data are presented as mean $\pm$ SD, n = 5 of all the animals in individual group. (Two-way ANOVA, Holm-Sidak post-hoc test, *$p < 0.05$, ***$p < 0.001$).

progression and metastasis (Massagué et al., 2000; Padua and Massagué, 2009). TGF-β1 is also known to utilize SMAD3 to inhibit CD16-mediated IFN-γ production, proliferation, and antibody-dependent cellular cytotoxicity in human natural killer (NK) cells (Trotta et al., 2008; Yu et al., 2006).

Recent advances in finding the small molecule inhibitors against TGF-β receptors and various other signaling molecules may empower us to modulate TGF-β signaling for consequent therapeutic interventions in cancer. Inhibiting TGF-β-induced signaling includes targeting ligand-receptor interactions, and this intracellular signaling is one major direction for cancer therapy (Neuzillet et al., 2015). LY2157299 monohydrate (galunisertib) is a recently developed small molecule inhibitor of TGF-βR1. Galunisertib binds at ATP-binding sites of the TGF-βR1, preventing the intracellular phosphorylation of SMAD2 and SMAD3 (Bhola et al., 2013; Bueno et al., 2008; Serova et al., 2015). Galunisertib has demonstrated tumoricidal activity in synergism with paclitaxel or sorafenib in xenograft models of breast or hepatocellular carcinoma (Bhola et al., 2013; Bueno et al., 2008; Joseph et al., 2013). Phase I studies have shown that galunisertib is safe in patients with advanced forms of solid tumors (Fujiwara et al., 2015; Rodón et al., 2015).

The central theme of the current work is to develop an immunotherapeutic protocol for targeting the microenvironment of primary tumors and/or metastatic areas, most notably by inhibiting the TGF-β receptors. TGF-β acts as a critical and dominant tumor suppressor cytokine opposing IL-15-mediated CD8⁺ T cell expansion and thus counteracting homeostatic dysregulation leading to malignant transformation (Lucas et al., 2006). TGF-β and IL-15 are engaged in opposing extrinsic signals to control and contract the clonal expansion of CD8⁺ T cells (Lucas et al., 2006; Sanjabi et al., 2009). In contrast, TGF-β and IL-15 play a synergistic role in promoting phenotype switch of NK cells to innate lymphoid cell suggesting considerable plasticity between them (Hawke et al., 2020). We have investigated the combined therapy of galunisertib and recombinant interleukin (rIL)-15-activated DCs against a highly metastatic and aggressive murine lymphoma called Dalton lymphoma (DL) (Hira et al., 2014; Klein and Klein, 1954). The main objective of the study is to formulate a novel therapeutic strategy in this experimental lymphoma similar to that of clinical conditions. Our data suggest that galunisertib alone is not sufficient for significant therapeutic benefits against the lymphoma. However, dual treatment with galunisertib + rIL15-activated DCs significantly enhanced the lifespan of the treated animals with nearly 80% survival compared with 100% death of the untreated group at day 60. CD4⁺ T cells (T_h) derived from the DL mice showed enormous increase in regulatory T cells (Tregs) in TDLN, which was obliterated in mice that received the dual therapy. Dual therapies in DL mice led to downregulation of Neuropilin-1 (Nrp-1) and increased the distribution of memory CD8⁺ T cells in the lymph node and in the lymphoid organs like spleen. Altogether, our data demonstrated that galunisertib treatment at a clinically relevant dose enhances the anti-tumor activity of rIL15-activated DC (rIL15 DC) resulting in robust enhancement of lifespan in lymphoma-bearing animals and is associated with enhanced T cell activation signatures in TDLN. These results further support the clinical relevance of targeting TGF-βRI in combination with adoptive cell therapy against lymphoma.

RESULTS

Adoptive Transfer of IL-15-Activated DC Synergizes with Galunisertib for Enhanced Antitumor Immunity against DL

We have studied a highly metastatic murine lymphoma model called Dalton lymphoma, grown as lymphosarcoma in the peritoneum (primary tumor site) of AKR/J mice to test our hypothesis. Tumoricidal effect of increasing concentrations of the galunisertib (LY2157299) was tested in DL tumor-bearing mice (Figure 1A).

Results showed a concentration-dependent reduction in abdominal circumference (tumor volume) in DL tumor-bearing mice, whereas untreated control had unrestricted tumor growth with large semisolid tumor mass in the abdomen (Figures 1B–1E, Table S1A). Galunisertib treatment successfully reduced the general body weight indicating significant reduction in tumor mass in the peritoneum, which accounts for the massive increase in body weight in DL tumor-bearing mice (Figure 1F). Reduction in tumor volume was also accompanied by the increased survival of the treated mice (Figure 1G). *In vitro* tumoricidal activities of galunisertib against DL tumor cells showed concentration-dependent growth inhibition with the highest inhibition recorded ~80% at 10 μM inhibitor concentration (Figure S1A). Similar anti-proliferative results were observed against 2PK3 and NIH/3T3 cells (Figures S1B and S1C).

Galunisertib-only treatment inhibits the tumor cells' growth *in vitro* significantly. However, *in vivo* treatment did not produce highly significant impact on the DL tumor-bearing mice with respect to survival or reduction in tumor size including the clearance of the tumor and recurrence. To get a better response, we introduced combined therapy of galunisertib and interleukin-15-activated splenic DCs against DL-bearing animals. *In vitro* growth inhibition of DL and 2PK3 cells was significantly inhibited in the presence of combined effect of naive and activated DCs. Among the cytokines, rIL15 has more pronounced effect compared with treatment with granulocyte-macrophage colony-stimulating factor (GM-CSF) (Figures S1D and S1E). Lipopolysaccharide (LPS)-treated DC was used as a positive control for DC activation. rIL15-activated DC also demonstrated significant cytotoxicity against galunisertib-treated DL or 2PK3 cells (Figures S1F and S1G). We have also tested concentration-dependent growth inhibition and cytotoxicity in galunisertib-treated DL tumor cells by naive (DC1), rIL15-activated (DC2), and LPS-activated (DC3) DCs (Figures S1H and S1I). This DC-mediated growth inhibition is mediated by TNF-α (Figure S1J). Furthermore, rIL15-activated DC induced greater apoptosis of DL cells suggesting that cytokine-activated DC acquired additional tumoricidal properties in killing the tumor cells following treatment with galunisertib (Figures S1K and S1L).

We extended our study on tumoricidal activity of galunisertib with or without human peripheral blood DC against a panel of human lymphoma cell lines. Our results suggest that human lymphoma cells are also susceptible to galunisertib in a concentration-dependent manner with wide range of IC_{50} values. IC_{50} values of galunisertib against Raji, THP-1, U937, and JE6.1 were recorded as 0.7763, 0.1085, 0.1240, and 0.1640 μM, respectively (Figures S2A–S2D). Following treatment with naive (GM-CSF DC) or activated (rIL15 DC or LPS DC) human peripheral blood DC, lower concentration of galunisertib (50 nM) demonstrated enhanced tumoricidal effect against all the cell lines tested (Figures S2E–S2H). Similar to the results in murine lymphoma cells, activated human DCs potentiate galunisertib-mediated tumoricidal effect against all the human lymphoma cells tested (Figure S2). rIL15-activated DC shows enhanced tumoricidal activity against Raji cells when used in combination with galunisertib (43.21 ± 1.6 versus 53.95 ± 6.92, n = 3, between rIL15 DC alone and combined treatment of rIL15 DC + galunisertib) (Figure S2E). We did not observe statistically significant effects between the two treatment schedules as judged by two-way ANOVA analysis. However, the quantitative data clearly showed that the combination treatment has an edge over the rIL15 DC-only treatment. Besides TGF-β receptor (TGF-βR), TGF-β has been reported to bind to the surface of some lymphoma B cells through interaction with heparan sulfate (HS) but not through the TGF-β receptor (Yang et al., 2013). These observations suggest that B lymphoma cells may adopt other default pathways with response to TGF-β signaling besides TGF-βR. This could be the likely reason for the less-than-optimum response of Raji cells compared with other cell lines tested in the experiment. We presume that the blocking of TGF-βR with lower concentration of galunisertib was unable to demonstrate significant tumoricidal activity against Raji cells due to paucity of the receptor and the presence of alternative HS signaling. Also, many B lymphoma cell lines differ in their sensitivity to TGF-β1-mediated growth suppression due to lack of functional TGF-βR (Chen et al., 2007). These results suggest that binary application of galunisertib and adoptive transfer of IL-15-activated DC could be effective for favorable outcome against human lymphoma.

Based on the above results, we have tested the effect of rIL15-activated DC in combination with galunisertib in DL tumor-bearing mice. Similar to the presentation above (Figure S1A), a combination therapy schedule was formulated involving rIL15-activated DC (1×10^6) plus galunisertib (10 mg/kg body weight) (Figure 1H). Data suggest that dual treatment selectively reduced the abdominal circumferences of the DL tumor-bearing animals significantly, compared with no treatment or treated with galunisertib alone (Figures 1I–1L). In addition to the abdominal volume (Table S1B), the body weight of the dual treated group was also reduced dramatically compared with untreated condition or animals treated with the inhibitor

alone (Figure 1M). Survival statistics also scored significantly higher with more animals surviving beyond day 40 (nearly 75%), whereas animals treated with inhibitor alone all died at day 40 and untreated animals died between days 20 and 22 (Figure 1N). Images presented in Figure 1O demonstrated the physical features of the treated animals (v) with nearly healthy-looking features similar to healthy control (i), whereas the untreated (ii), inhibitor- (iii) or rIL15 DC-only-treated groups (iv) showing distinct recognizable bulge in the abdominal areas. Galunisertib appears to have dramatic impact on the size of the lymph nodes as well as on lymphoid organs like spleen when given in combination with rIL15-activated DC (Figure 1O). In contrast to IL-15-activated DC, naive unactivated DC alone or in combination with galunisertib is significantly less tumoricidal against the established DL tumor (Figure S3). The lack of anti-tumor potential of DC alone is reflected in continuous tumor growth and inability to improve the survival of the animals following treatment (Figures S3A–S3C). These results suggest that adoptive transfer of IL-15-activated DC has rate-limiting effect against the disease-exacerbating factors in lymphoma. We also looked in to the anti- and pro-inflammatory cytokine profiles of the treated groups to correlate the therapeutic outcome with the involvement of cytokine generation. Our data suggest that serum IFN-γ goes high in dual treated group, and hits the bottom in DL tumor-bearing animals (Figure 1P). This indicates that IFN-γ acts as a healer mechanism for the dual therapy. In contrast, TGF-β level shoots up in DL tumor-bearing animals, which comes down to basal level with successful cellular therapy in combination with chemotherapy (Figure 1Q).

Downregulation of FOXP3 in CD4$^+$ T Cells Coincides with Successful Dual Therapy

Abolition of TGF-β in the serum of the dual treated group prompted us to investigate the role of Tregs in TDLN and vascularized organs like the liver, lung, and spleen where metastasis was observed. Histopathological analysis of the liver, lung, or spleen distinctly showed extensive metastasis with tumor cells, whereas the treated group appears to have cleared large portion of such infiltration (Figures S4A–S4C). Quantitative estimation of tumor foci in liver demonstrated significant difference in the number of metastatic foci between untreated and combined treatment group (Figure S4D). During tumor advancement and before metastasis, TDLN goes through many additional extensive modifications leading to invasion by tumor cells, borrowed from the primary sites. Such transformations include increased lymph node angiogenesis, remodeling of the blood vessel, and increased secretion of chemokine and cytokine. These events ultimately lead to changes in the composition of immune cells, resulting in a "tumor-abetting" microenvironment or the pre-metastatic niche. In the lymph node architecture, perceptible changes were observed between untreated and dual treated animals with the latter showing the clearance of the tumor cell from core of the lymph node, leaving very few tumor cells (Figure S4E).

We looked at the possible connection between the clearance of the tumor cells and the alteration of FOXP3$^+$ Tregs in the T$_h$ cells repertoire. Immunohistochemical analysis suggests wide distribution of CD4$^+$ T cells in the TDLN section metastasized by the tumor cells with proportional increase in the FOXP3$^+$ cells (Figures 2A and 2B). Quantitative estimation indicates that CD4$^+$ T cells were overwhelmed in the nodal architecture of DL mouse, which noticeably diminished in the dual treated group with an intermediate level of effect observed in galunisertib only-treated group (Figure 2C). FOXP3$^+$ Tregs have extensive distribution in DL tumor-bearing nodes, which greatly reduced in the dual treated group (Figure 2D). We also looked into the correlation between the CD4$^+$ T cells and FOXP3$^+$ Tregs in the nodal architecture. Data suggest that most of the recorded CD4$^+$ T cells are of FOXP3$^+$ Tregs phenotype with high correlation coefficient (r) value (0.96), which diminished significantly in dual treated group (0.53) (Figures 2E–2H). We also looked at the CD4$^+$CD25$^+$FOXP3$^+$ population in the TDLN T cells between untreated DL mice and DL mice treated with the dual therapy. In the spleen, CD4$^+$CD25$^+$ cells were reduced from 19.4% in DL mouse to 11.4% in animals treated with combination therapy. Galunisertib-only treatment had intermediate effect. CD25$^+$FOXP3$^+$ cells showed significant surge (67%) in the untreated DL mice, which reduced to less than 1% in mice receiving dual therapy (Figures 2I and 2J). We observed similar pattern in the splenic FOXP3$^+$-positive CD4$^+$ T cells suggesting critical role of Tregs in the disease pathogenesis (Figure S5).

Occlusion of Treg Cells Is Associated with the Disappearance of Neuropilin-1 following Galunisertib Treatment

Nrp-1 is expressed on Treg cells, inducible by FOXP3 expression (Hill et al., 2007). Nrp-1 forms receptor complexes with some members of the plexin-A family, which deliver semaphoring signals, necessary for axon guidance in the nervous system. The interactions and association of semaphorins and their cognitive receptors are also known to be involved in immune responses (Suzuki et al., 2008). Sarris et al. (2008) showed that antibody-mediated blockade of Nrp-1 reduces the number of extensive interactions between Treg cells and DC (Sarris
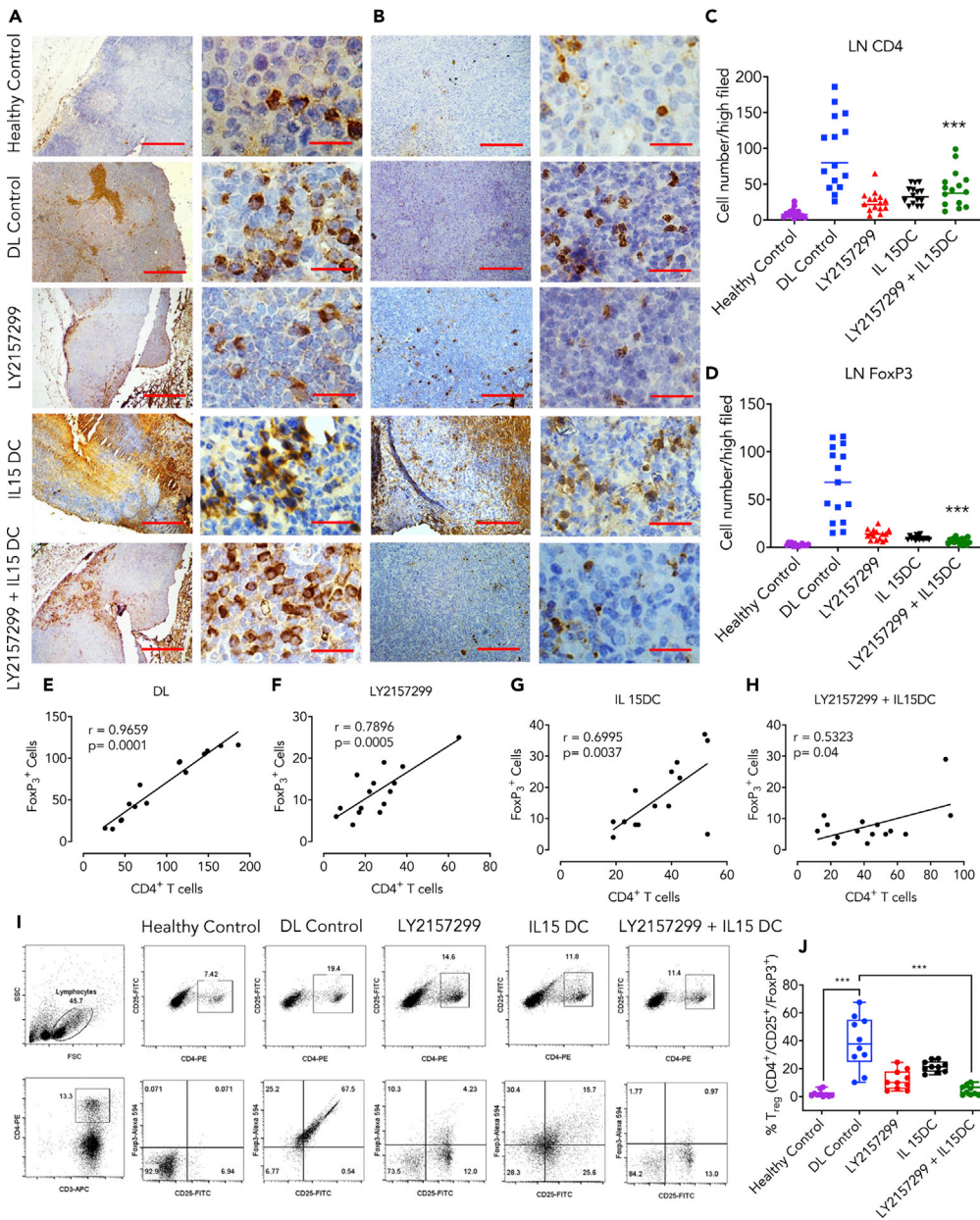
Figure 2. Ablation of CD4$^+$CD25$^+$FOXP3$^+$ Treg Cells Contributes to Tumoricidal Effect of Galunisertib + rIL15 DC in Mice with DL Tumor

(A and B) Immunohistochemical localization of CD4$^+$ T (A) and FOXP3$^+$ Treg cells (B) in the lymph node of healthy control, DL tumor-bearing, galunisertib alone-, rIL15 DC only-, or galunisertib + rIL15 DC-treated animals (100× and 400× magnification). Scale bar, 50 μm.

(C–E) Quantitative estimation of CD4$^+$T cells (C) and FOXP3$^+$ Treg cells (D) in the lymph nodes following indicated treatment. Linear regression analysis for the relationship of CD4:FOXP3 ratios in the lymph nodes (LN) of the untreated DL (r = 0.9659; p = 0.0001) (E). Values are mean ± SD, two-way ANOVA, Holm-Sidak post-hoc test, ***p < 0.001.

(F–J) Galunisertib-treated (r = 0.7896; p = 0.0005) (F), rIL15 DC-treated (r = 0.6995; p = 0.0037) (G), and galunisertib + rIL15 DC-treated groups (r = 0.5323; p = 0.04) (H). Percentage of CD4$^+$/CD25$^+$T cells in the gated lymphocytes (upper panel) and CD25$^+$/FOXP3$^+$ T cells in the gated CD3$^+$/CD4$^+$T cells (lower panel) (I). Absolute numbers of CD4$^+$/CD25$^+$/FOXP3$^+$ Treg cells in the LN following indicated therapy (J). Data are presented as mean ± SD, n = 5, two-way ANOVA, Holm-Sidak post-hoc test, ***p < 0.001.

et al., 2008). Furthermore, retroviral introduction of Nrp-1 armed Th cells with an ability to have significant potential of interactions with immature DC. Our results demonstrated that galunisertib treatment substantially reduced the Nrp-1 expression in Treg cells, which was significantly enhanced following binary challenge against the DL tumor (Figures 3A and 3B). Surface expression of Nrp-1 on Tregs was markedly reduced in dual treatment condition (Figures 3C and 3D). We also looked at the induced Treg/natural Treg cell ratio in the DL mice and compared with the treated groups either with galunisertib or galunisertib + rIL15 DC. Induced Tregs were found to be increased from negligible in healthy control (0.33%) to 10.3% in DL group, which declined nearly to the same level (0.66%) of healthy control in dual treated animals (Figures 3E and 3F). Binary challenge with galunisertib plus rIL15-activated DC limits the FOXP3-positive Tregs and downregulates the TGF-β synthesis and upregulates IFN-γ, compared with the DL mice (Figures 3G and 3H).

Combined Treatment Elaborates CD8^{+} T Cells with Memory Phenotype in Lymph Node Architecture

Results from the earlier sections established the rational and logic to look at the distribution of CD8^{+} T cells in lymph node in untreated and treated DL animals. Data suggest a dramatic reduction of CD8^{+} T cells in the lymph node in untreated animals, which was significantly increased following binary challenge of galunisertib and activated DC. Only galunisertib treatment also boosted the CD8^{+} T cells in the nodal architecture (Figure 4A). CD8^{+} T cells increased rapidly and become prominent in the lymph node with increased number, percentage, and higher CD3^{+}/CD8^{+} ratios (Figures 4B–4D). Similar trend was observed in the spleen with significant expansion of CD8^{+} T cells (Figures 4E–4H).

To show the memory phenotype of the infiltrating CD8^{+} T cells in the lymph node and the spleen of the treated organ, we performed immunohistochemical analysis of lymph node and splenic section. CD62L expression in the lymph node markedly increased following treatment with galunisertib or galunisertib + rIL15 DC (Figures 5A and 5B). This was also accompanied by the emergence of positive correlation between the abundance of CD8^{+} T cells and higher expression of memory phenotype, CD62L, in the same cell population (Figures 5C–5F). CD8^{+} T cells gated on the CD3^{+} T cells followed by dual staining with CD44 versus CD62L indicated a complete shift toward the expression of adhesion receptor CD44. Isoforms of CD44 were widely and asymmetrically expressed in breast carcinoma and are correlated with the tumor subtypes and cancer stem cell markers besides similar roles in other types of cancer (Chen et al., 2018; Ponta et al., 2003; Zöller, 2011). Our results suggested that following treatment with galunisertib + rIL15-activated DC, T cells express CD62L, which were nearly absent in untreated DL mice (Figure 5G).

We also compared the percentage of effector memory T cells (T$_{EM}$ **cells**) and central memory T cells (T$_{CM}$ **cells**), based on the differential expression of selectin. Both CD4^{+} and CD8^{+} T cells have two main subclasses of memory cells: central-memory (T$_{CM}$) and effector-memory (T$_{EM}$) T cells (Sallusto et al., 2004). T$_{CM}$ cells are generally identified as cells expressing high levels of the IL-7 receptor (CD127), C-C chemokine receptor type 7 (CCR7), and adhesion markers, viz., CD44 and CD62L, and low levels of killer cell lectin-like receptor subfamily G member 1 (KLRG-1). In addition, T$_{CM}$ cells are characterized by their increasing and intensified potential for proliferation following antigen encounter in recall response. T$_{EM}$ cells are phenotypically different from T$_{CM}$ cells, and they generally express low levels of CD62L and CD127, high levels of KLRG-1, and are deficient in CCR7. In contrast to T$_{CM}$ cells, T$_{EM}$ cells manifest quick and extensive effector functions involving production of granzyme B and IFN-γ, although they have a limited potential of proliferative response. Elevated levels of CD62L and CCR7 expression allow the T$_{CM}$ cells for preferential homing to secondary lymphoid organs producing CCR7 ligands CCL19 and CCL21, and thus are well placed to protect from a systemic infection and provide repertoire of fresh brigade of effector cells to the peripheral tissues following stimulation. In contrast, lack of CCR7 and CD62L expression in T$_{EM}$ cell results in its trafficking through the non-lymphoid tissues (Jameson and Masopust, 2009). Our results suggest that in DL tumor-bearing animals, splenic T cells consist of T$_{EM}$ type with low expression of CD62L, which further reduced significantly by treatment with galunisertib alone and was more pronounced following binary effect of galunisertib + rIL15-activated DC (Figure 5H). In contrast, galunisertib + rIL15 DC-treated mice had a population of T$_{CM}$ cells and the DL tumor-bearing animals have very low or no CD62L expression (Figure 5I). Although CD8^{+} T$_{CM}$ and T$_{EM}$ cells are generated in human and mice, tumor-reactive CD8^{+} T$_{CM}$ cells are appearing to be superior compared with their effector memory (T$_{EM}$) counterpart. T$_{CM}$ cells turn out to be a superior mediator for therapeutic response compared with T$_{EM}$ cells with enhancement in homing to lymphoid tissues (Klebanoff et al., 2005). Following antigen recognition, wandering T$_{CM}$ cells undergo rapid and robust proliferation and differentiate into effector cells and then migrate to secondary
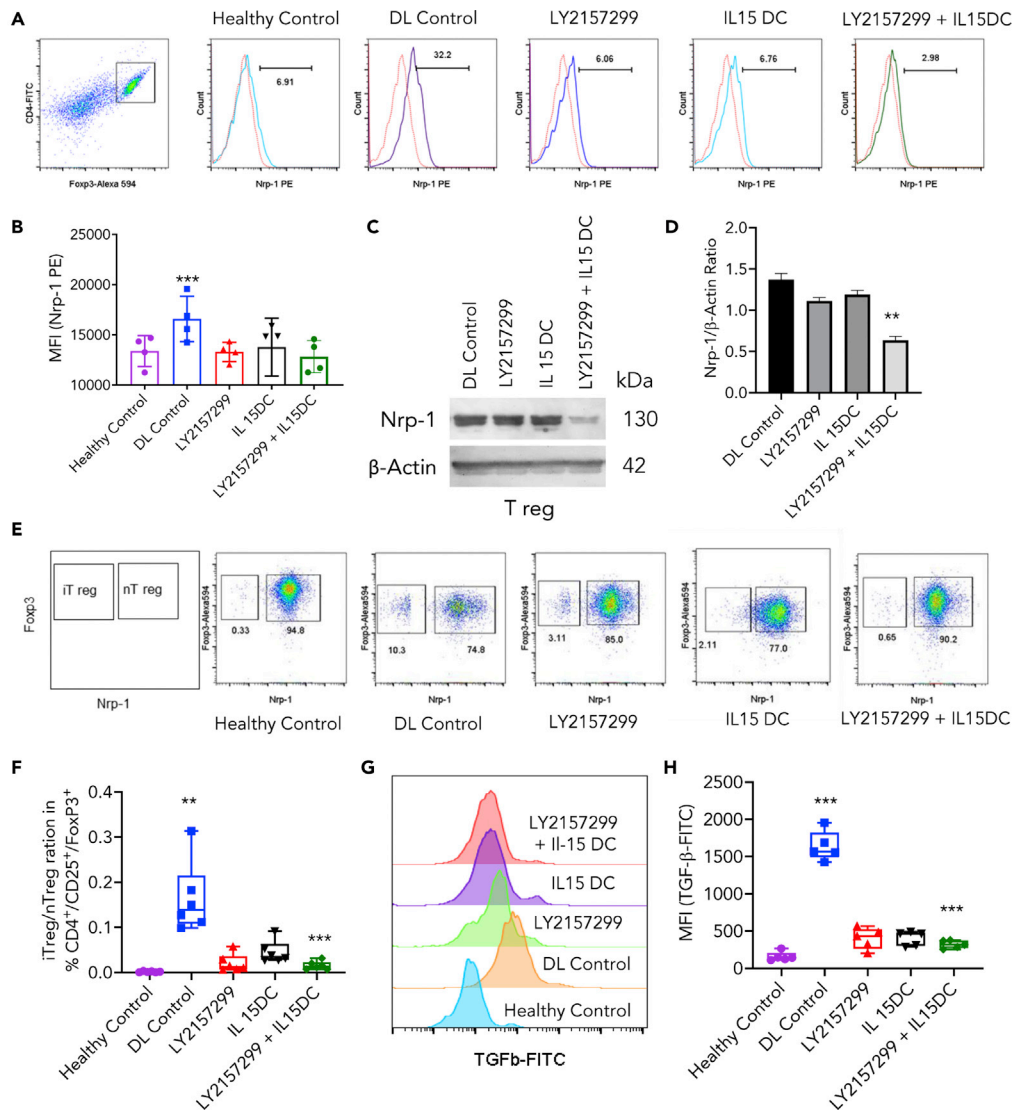
Figure 3. TGF-β/FOXP3-Specific Ablation of Nrp-1 Expression in Mice Treated with Galunisertib and Adoptively Transferred rIL15-Activated DC Impaired the Tumor Growth

(A and B) Sorted CD4$^+$FOXP3$^+$ Treg cells from the healthy, untreated, or indicated treated groups were stained with anti-mouse Neuropilin-1 (Nrp-1) antibody (R&D systems) for analysis (histogram and quantization of mean fluorescence intensities) by flow cytometry. Representative histograms from one experiment out of three with similar results are shown. Values are mean ± SD, n = 3, two-way ANOVA, Holm-Sidak post-hoc test, **p < 0.01.

(C and D) Western blot analysis of Nrp-1 expression and its fold increase or decrease corresponds to the internal control in sorted CD4$^+$FOXP3$^+$ Treg cells in DL tumor-bearing mice either untreated or treated with galunisertib, rIL15 DC, or galunisertib + rIL15 DC. Values are mean ± SD, n = 3, two-way ANOVA, Holm-Sidak post-hoc test, **p < 0.01.

(E and F) Percent analysis of inducible versus natural Treg cells in the lymph node population in healthy control, DL tumor-bearing, and treated animals. Representative example of dot plot from three experiments is shown. Values are mean ± SD, n = 3, two-way ANOVA, Holm-Sidak post-hoc test, **p < 0.01.

(G and H) Histogram and mean fluorescence intensity analysis of TGF-β in the sorted CD4$^+$CD25$^+$FOXP3$^+$ Treg cells. One representative of four similar experiments performed. Values are mean ± SD, n = 4, two-way ANOVA, Holm-Sidak post-hoc test, ***p < 0.001.

lymphoid organ by virtue of abundant homing receptors (von Andrian and Mackay, 2000). Critical lacking of lymph node homing receptor paralyzes the potential of the T$_{EM}$ cells in spite of their capability for rapid cytolysis of infected cells and only recirculate between the nonlymphoid tissues and peripheral blood (Klebanoff et al., 2005; Sallusto et al., 1999). These potential drawbacks of T$_{EM}$ cells are likely responsible for
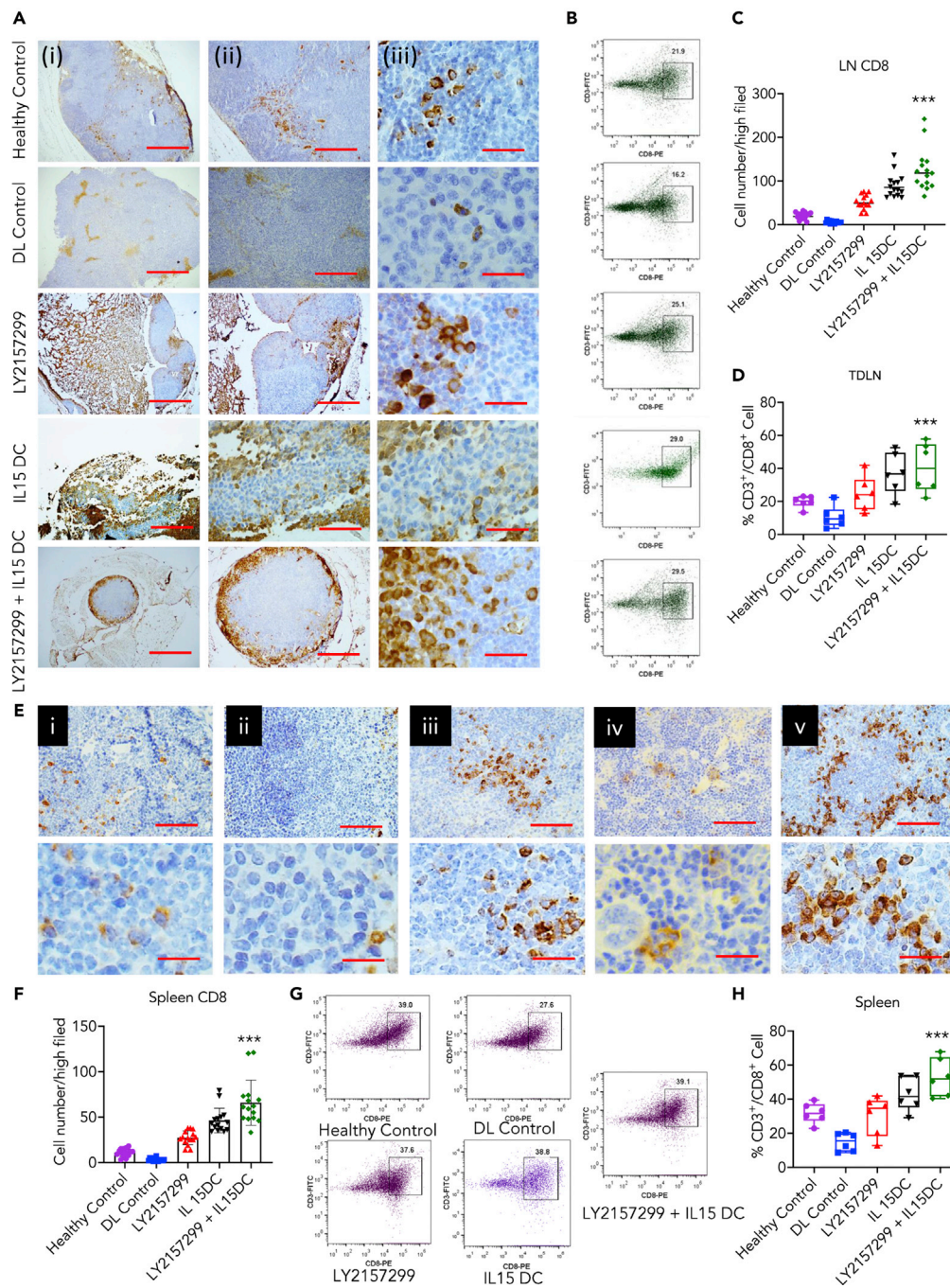
Figure 4. Increased Numbers of Highly Activated CD8+ T Cells in the Tumor-Draining Lymph Nodes (TDLN) Predicts Better Prognosis following Adoptive Transfer of Activated DC

(A) Immunohistochemical analysis of expanding lymph node CD8+ T cells in galunisertib + rIL15 DC-treated animals when compared with healthy control, untreated DL, or rIL15 DC-treated mice (40× (i), 100× (ii), and 400× (iii) magnification). Scale bar, 50 μm.

(B) Dot plot analysis for CD3+/CD8+ T cells in the galunisertib + rIL15 DC-treated animals compared with untreated group.

(C–H) (C) Quantitative estimation and (D) % positive CD8+T cells in the lymph nodes following indicated treatment. (E–H) Identical experiments with splenic CD8+ T cells from the above groups. Data from one experiment out of five (n = 5) with similar results. Two-way ANOVA, Holm-Sidak post-hoc test, ***p < 0.001.
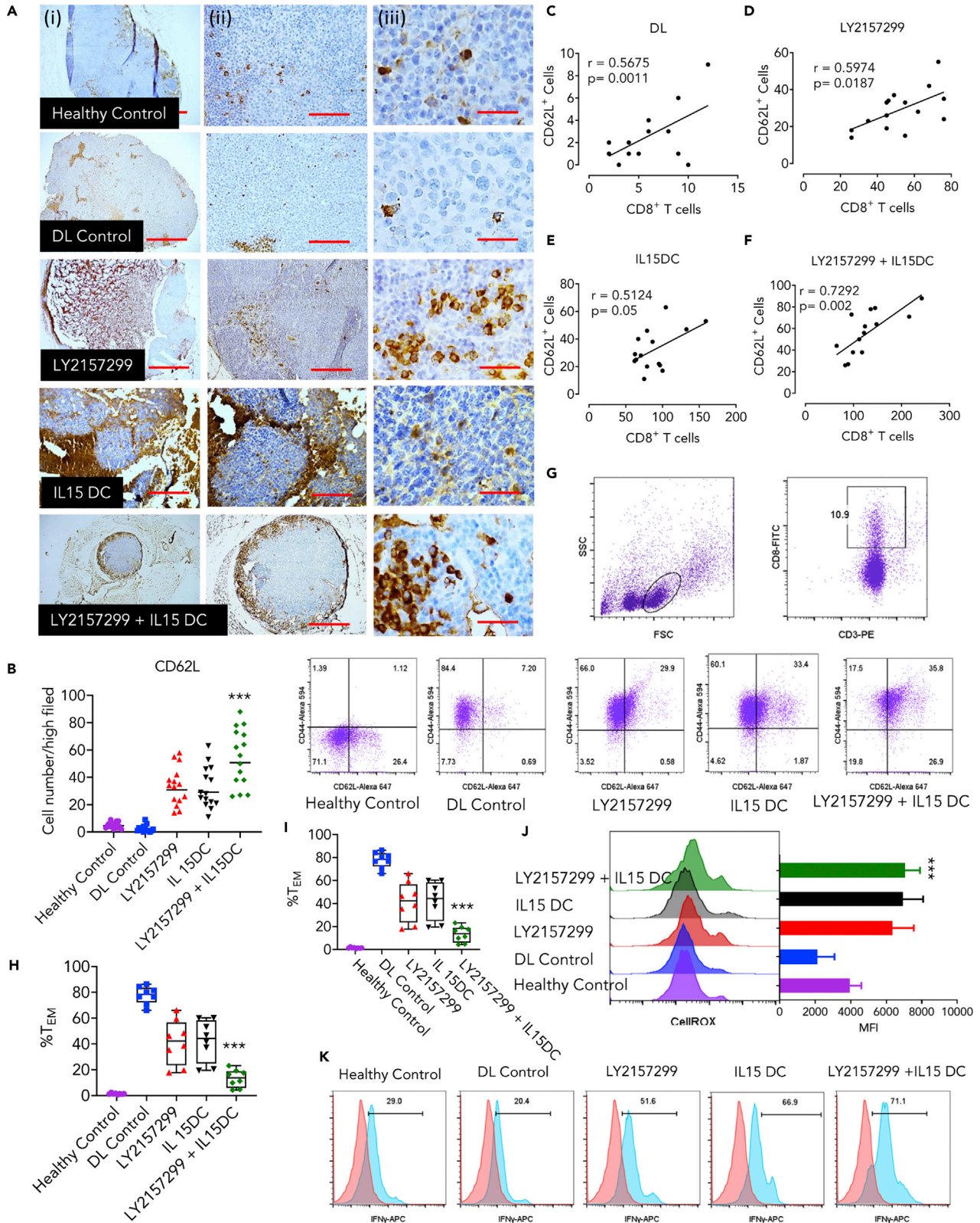
Figure 5. Expansion of CD62L-Positive Central Memory T Cells in Mice Treated with Galunisertib + rIL15-Activated DC with Enhanced Secretion of IFN-γ

(A–F) (A and B) Immunohistochemical localization of CD62L cells in TDLN of galunisertib + rIL15 DC-treated animals compared with untreated DL group and animals treated with galunisertib and rIL15 DC only (40× (i), 100× (ii) and 400× (iii) magnification). Scale bar, 50 μm. Linear regression analysis for the relationship of $CD8^+:CD62L^+$ cells in the LN architecture of treated and untreated groups (C) DL (r = 0.5675; p = 0.0011), (D) galunisertib only (r = 0.5974; p = 0.0187), (E) rIL15 DC only (r = 0.5124; p = 0.05), and (F) galunisertib + rIL15 DC (r = 0.7292; p = 0.002).

(G) Analysis of $CD44^+/CD62L^+$ memory T cells gated on $CD3^+/CD8^+$ T cells obtained from galunisertib + rIL15 DC-treated animals and compared with untreated DL mice or galunisertib-treated group.

(H and I) Quantitative estimation of percent effector and central memory T cells, based on the expression of CD44 and CD62L. Data are presented as mean ± SD, n = 5, two-way ANOVA, Holm-Sidak post-hoc test ***p < 0.001.

(J) Generation of reactive oxygen species (ROS) in response to therapy promotes T cell activation and proliferation, based on staining with CellRoxGreen (Invitrogen). Data are presented as mean ± SD, n = 4, two-way ANOVA, Holm-Sidak post-hoc test, ***p < 0.001.

(K) Enhanced production of IFN-γ by CTLs derived from the DL mice treated with galunisertib + rIL15 DC as depicted by histogram analysis. Representative data of one experiment out of four (n = 4) similar experiments is shown.

their lack of participation in tumoricidal response, whereas the bold T_{CM} cells demonstrate durable and persistent antitumor potential (Figure 5). **CellROX** Green reagent, a novel fluorogenic probe for measuring the oxidative stress, was used in the live cells. The cell-permeant dye produced weak fluorescence in reduced state and exhibited bright green photostable fluorescence upon oxidation by reactive oxygen species (ROS). $CD8^+$ T cells derived from the DL tumor-bearing mice have very low ROS activity, whereas cells derived from the treated groups have high ROS activity. Significant difference was observed in mean ROS activity in galunisertib or galunisertib + rIL15 DC-treated animals (Figure 5J). Also, the T cells derived from galunisertib-treated animals have significantly higher number of IFN-γ (52%) compared with that of DL mouse. Galunisertib + rIL15 DC-treated animals produced significantly more IFN-γ (71%) suggesting an important contribution of memory $CD8^+$ T cells for the therapeutic success (Figure 5K).

PD-I Status in $CD8^+$ T Cells Associates with Survival and Therapeutic Outcome

We assessed the expression of PD-1 in $CD8^+$ T cells in paraffin-embedded tissue sections derived from galunisertib + rIL15 DC-treated animals and compared with healthy control, untreated DL, galunisertib, or IL-15 DC-treated mice. Immunofluorescence with antibodies specific to mouse PD-1 (Clone 29F.1A12) and CD8 (Clone 53–6.7) were used where cells expressing $CD8^+$ (red), $PD-1^+$ (green), and DAPI for nuclei (blue) were analyzed. Colocalization scatterplot corresponding to the indicated treatment is shown in Figure 6A. The results of fluorescence colocalization study were also presented graphically where the intensity of $CD8^+$ and $PD-1^+$ cells was plotted for each pixel, similar to the output provided for flow cytometry data (Figure 6B). Additional insights from scatterplot colocalization studies include identification of populations of distinct compartments. Pearson's correlation coefficient was used for quantifying the colocalization efficiency. The data show that in TDLN % of $CD8^+$ cell reduced to negligible in DL and restores only after the dual therapy. Percent $PD-1^+$ cells were high in untreated (DL) and in LY2157299- or IL-15 DC-treated groups but less in healthy control as well as in dual treated groups (Figure 6B). Double-positive cells ($CD8^+$, $PD-1^+$) were significantly higher in case of DL and LY2157299 groups, whereas treatment with IL-15DC or IL-15DC + LY2157299 showed significant reduction in percent dual-positive cells (Figure 6B). For automated counting, Image-Pro software allows cell segmentation, based on DAPI staining of the nucleus and morphometric characteristics (middle). An automated count was performed, which generated regions of interest (ROI) corresponding to $CD8^+$ T cells co-expressing PD-1. ROI corresponding to $CD8^+$ T cells expressing PD-1 were recorded (original magnification, ×400), and quantitative estimation of percent $PD-1^+$ and $CD8^+$ T cells is presented in bar diagram (Figure 6C). Trendline of % positive $CD8^+$, $PD-1^+$, and dual-positive cells among the different treatment groups based on scattered plot analysis is presented in Figure 6D. Intensity of PD-1 expression in CD8 cells is shown as histogram plot for the indicated treatment group, and the mean fluorescence intensity is presented in bar graph (Figure 6E). Data show that PD-1 expression escalated in LY2157299- and rIL15 DC-treated groups, whereas in binary treatment group, it is reduced significantly. Lack of $CD8^+$ T cells in the lymph node of untreated DL mice led to disease exacerbation, which was significantly reduced following dual treatment assisted by abundance of $CD8^+$ T cells. PD-1-expressing T cells in the lymph node of treated animals likely undergo senescence and death following clearance of the malignant cells.

Successful Combination Therapy Obliterates SMAD Phosphorylation in Lymph Node Cells and Restores Immunity

The physiological outcome in TGF-β stimulation is diverse, and activation of TGF-β receptors initiates both SMAD-dependent and SMAD-independent signaling events (Derynck and Zhang, 2003). SMAD proteins transduce signals from TGF-β superfamily ligands that regulate cell proliferation, differentiation, and death
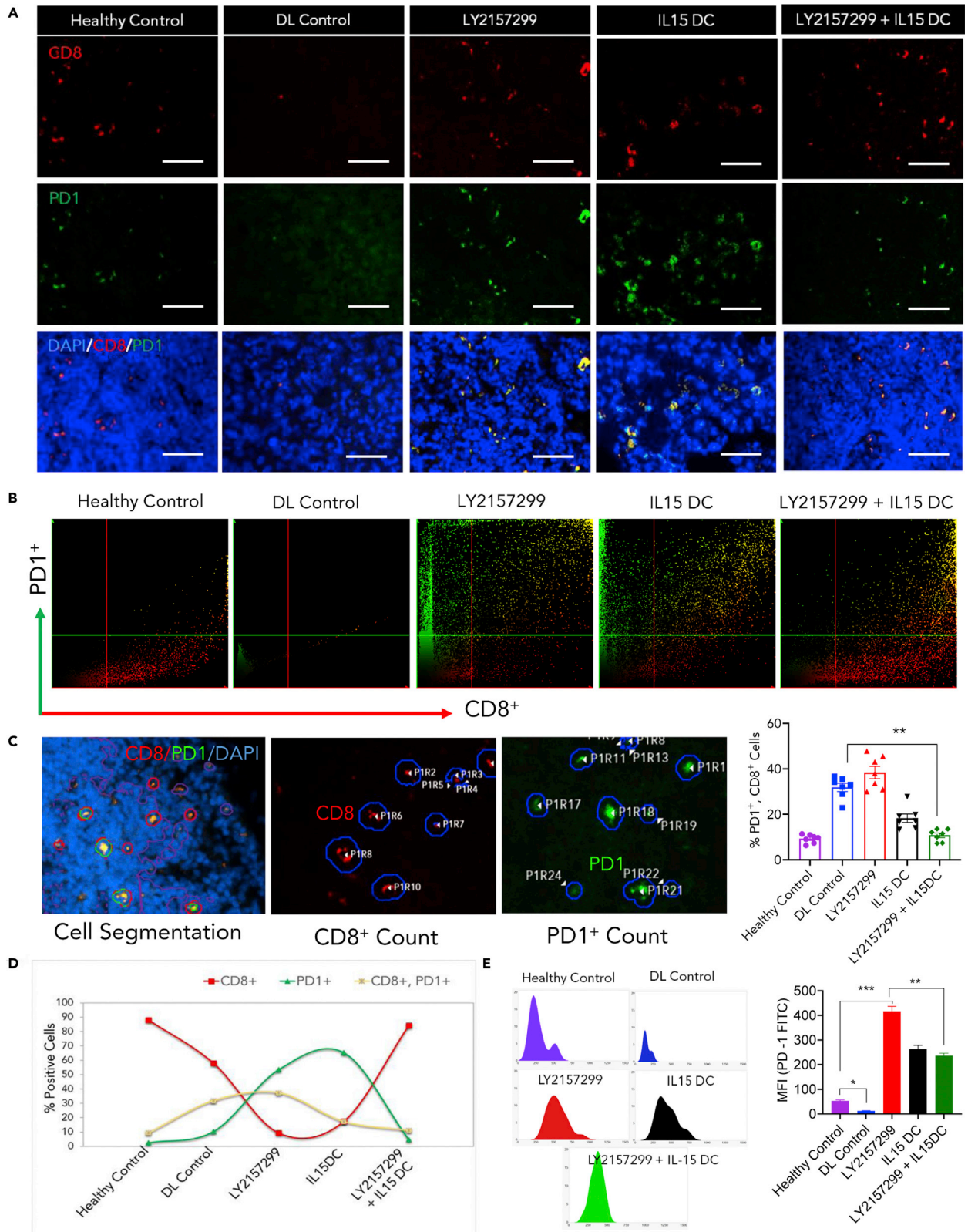
Figure 6. PD-1 Expression in Tumor-Draining Lymph Node-Infiltrating CD3$^+$CD8$^+$ T Cells

(A) Paraffin-embedded tissue sections derived from healthy control mice, untreated DL mice, or mice treated with galunisertib or rIL15 DC only or galunisertib + rIL15 DC were stained anti-mouse PD-1 (green) and counterstained with anti-mouse CD8 (red) and DAPI for nuclei (blue). Colocalization of these two markers was detected by merging the mono-staining pictures. Staining with isotype controls was included for each experiment (n = 9). Scale bar, 50 μm.

(B) The colocalization scatterplot corresponds to the events as shown in (A) (n = 7).

(C) Automated counting with Image-Pro software allows cell segmentation based on DAPI staining of the nucleus and morphometric characteristics (middle). Automated counting was performed, which generated regions of interest (ROI) corresponding to CD8$^+$ T cells co-expressing PD-1. ROI corresponding to CD8$^+$ T cells expressing PD-1 were recorded (original magnification, ×400), and quantitative estimation of percent PD-1$^+$ and CD8$^+$T cells is presented in bar graph (n = 7).

(D) Line graph represents the trendline of % single positive and dual positive cells in the treatment groups (n = 4).

(E) Quantitative mean fluorescence intensity estimation of PD-1$^+$-expressing cells in TDLN (n = 14). Data are presented as mean ± SD, n = 14, two-way ANOVA, Holm-Sidak post-hoc test, *p < 0.05, **p < 0.01, ***p < 0.001.

through activation of receptor serine/threonine kinases (Heldin et al., 1997; Heldin and Moustakas, 2012; Yang and Moses, 2008). Deregulation of TGF-β signaling leads to developmental anomalies and disease, whereas enhanced TGF-β signaling contributes to cancer and fibrosis (Derynck and Budi, 2019). SMAD phosphorylation (pSMAD) of receptor-activated SMAD (R-SMAD) led to the formation of complexes with the common mediator SMAD (Co-SMAD), which are imported to the nucleus where it binds to DNA and associates with transcription factors to regulate the expression of target genes. We looked at the effects of TGF-β stimulation on pSMAD expression in DL cells. Data suggest that tumor cells treated with TGF-β escalate the phosphorylation of SMAD, which was quickly obliterated in the presence of increasing concentration of galunisertib (Figure S6). TGF-β stimulates the growth of DL cells in a time-dependent manner suggesting that the DL cells respond to the TGF-β-mediated cell proliferation (Figures S7A and S7B). We used TGF-β-responsive cell lines like 2PK3, YAC-1, CT-26, and NIH/3T3 for comparison (Figures S7A and S7B). We then looked at the expression of TGF-β RI/RII and SMAD in DL besides in other cell lines as mentioned above. DL cells showed the expression of TGF-β RI/RII as well as SMAD 2/3 and SMAD 4 comparable to other cell lines tested (Figure S7C). DL cells responded to recombinant TGF-β stimulation with upregulation in phosphorylation of SMAD 2/3 in a concentration-dependent manner (Figures S7D and S7E). Phosphorylation of SMAD in DL cells under serum starvation was inhibited by increasing concentrations of galunisertib treatment. TGF-β stimulation upregulates the expression of pSMAD after 5 h of treatment, which was also blocked by galunisertib (Figures S7F–S7I).

Phosphorylation of SMAD was assessed in lymph node cells derived from untreated and treated animals for direct comparisons. Lymph nodes from the untreated DL mice showed extensive staining for pSMAD, which disappear in animals treated with galunisertib or galunisertib + rIL15 DC (Figure 7A). Cell number count in the areas of pSMAD-staining areas indicated a significant increase in untreated DL tumor-bearing animals compared with either galunisertib or galunisertib + rIL15 DC treatment (Figure 7B). Galunisertib + rIL15 DC combination therapy performed markedly better compared with galunisertib alone in restricting the phosphorylation of SMAD (Figure 7B). In case of spleen, we observed similar type of results as presented in TDLN (Figures 7C and 7D).

The above results on the success of the combination therapy also reflected in the restoration of immune responses in treated animals. Besides vastly changing the cellular topography in the tumor-bearing mice, CD4$^+$ T cells in spleen demonstrated antigen-specific proliferation, derived from the animals receiving dual therapy. We also looked into the potential of CD8$^+$ T cells in direct killing of the target cells. CD8$^+$ T cells from tumor-bearing mice were physiologically impaired with respect to cytotoxicity against the DL target cells. CD8$^+$ T cells from the animals treated with galunisertib plus rIL15-activated DC restored the potential and augmented the cytotoxicity against the DL tumor cells significantly (Figure S8). Besides T cells, DC also had substantial improvement in its functional aspects, which is obviously related to the improved immune responses in the treated group. CD11c$^+$/Class II$^+$ DC, derived from the animals treated with combination therapy, was substantially improved in lymph node and spleen compared with untreated littermate (Figures S9A–S9D). Expression class II and co-stimulatory molecules like CD40/CD80/CD86 showed significant upregulation in DC derived from the animals that received dual treatment compared with the untreated DL mice. The upregulation of the aforementioned molecules explains the improved and prodigious immune responses in tumor-bearing animals that received dual therapy (Figure S9E). Intracellular TNF-α expression in DC was also assessed to show the cytokine that regulates the effector functions of DC for tumor immunity. TNF-α expression in DC from the treated group increased substantially, which was greatly depressed in DL mice (Figure S9F). Enhanced immune functions of DC were also evident in
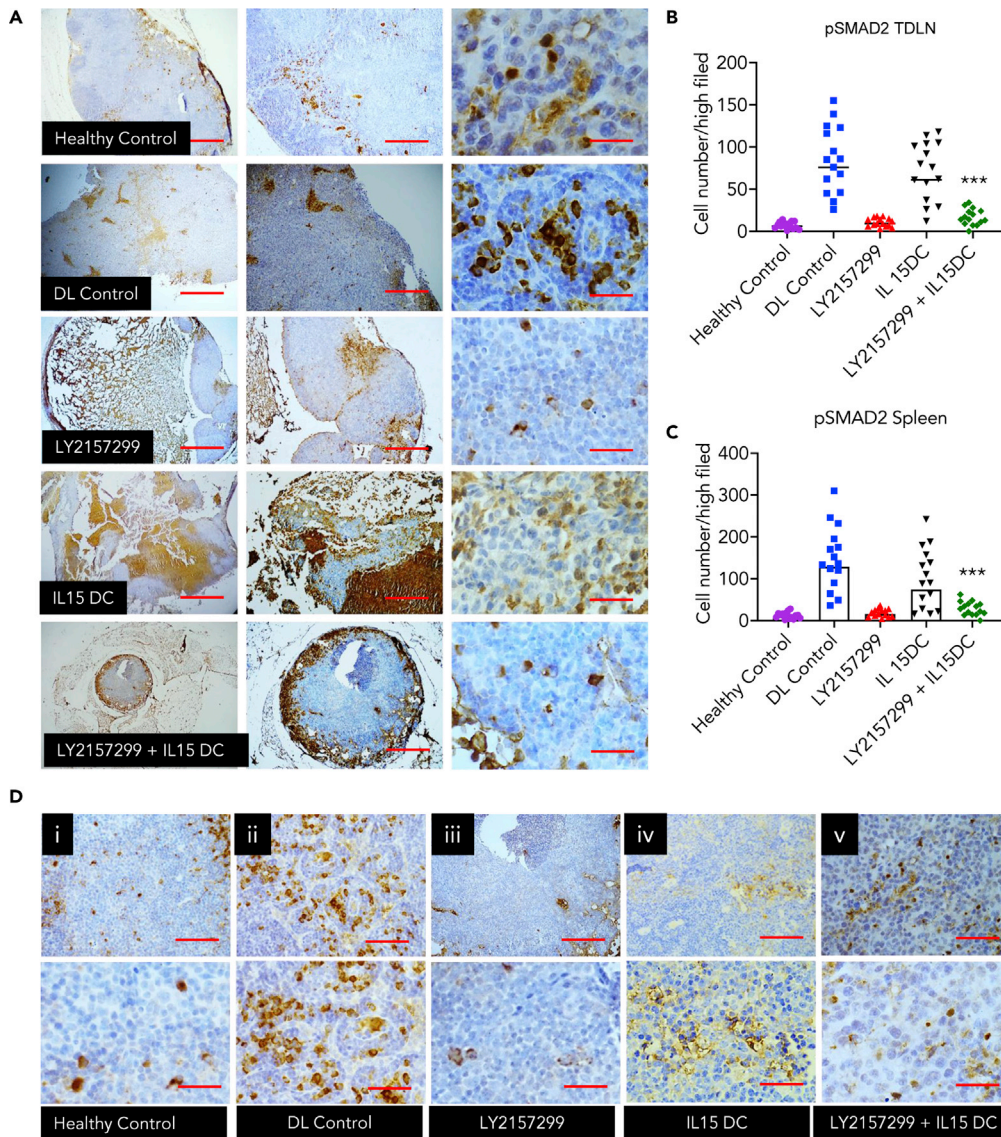
Figure 7. Downregulation of SMAD Phosphorylation in TDLN and Spleen Correlates with the Ablation of Nrp-1 and Regulatory T Cells following Dual Therapy

(A) Immunohistochemical localization of pSMAD2 in the tumor cells derived from the lymph node treated with galunisertib alone, rIL15 DC only, or galunisertib + rIL15 DC and compared with the untreated DL tumor-bearing condition (40× (i), 100× (ii), and 400× (iii) magnification). Scale bar, 50 μm.

(B) Quantification of the pSMAD2-positive cells in the TDLN based on the observation made in (A).

(C and D) Distribution of pSMAD-positive cells in the spleen as performed in A and B (100× and 400× magnification). Representative of one experiment of three similar experiment performed (data are presented as mean ± SD, n = 3, two-way ANOVA, Holm-Sidak post-hoc test, ***p < 0.001).

cytotoxic potential against the DL tumor cells. Effector function of DC derived from animals treated with binary combination was also restored with enhanced cytotoxicity against DL tumor cells. Effector DC (CD8^{+} killer DC) from the spleen of the treated animals demonstrated significantly higher cytotoxicity against the target cells (~30%) compared with <5% in DC derived from the untreated DL mice (Figure S9G). TNF-α also has its substantial presence in the serum of galunisertib + rIL15 DC-treated animals, significantly higher compared with untreated DL or galunisertib-only-treated animals (Figure S10). A rapid surge in serum TNF-α level was observed in galunisertib + rIL15 DC-treated animals from day 16 post tumor transplant when the cytokine level plummeted in untreated DL mice (Figures S10A–S10C). At day 24, when all the

untreated DL animals succumbed to death, serum TNF-α level in galunisertib + rIL15 DC-treated animals scored significantly high levels suggesting important role of this pleotropic cytokine in immune defense against the disease (Figure S10D). The cytokine level was maintained with slight reduction in subsequent days of assessment (Figures S10E and S10F). Antigen specific CD4$^+$ T cells (responder cells) derived from the animals treated with combination therapy demonstrated increased proliferation compared with the cells derived from DL mice (Figure S11). These results suggest that binary application of galunisertib + rIL15 DC significantly improved the immune responses in animals with metastatic lymphoma.

Linear Discriminant and Principal-Component Analysis for the Prediction of Biomarker

Linear discriminant analysis (LDA) and principal-component analysis (PCA) identify that Treg fragility and Th1-type immune responses are the potential predictive biomarkers for long-term immune protection of combined immunotherapy with galunisertib plus rIL15-activated DC. Results shown in Figures S2, 3, and 5 indicated that multiple arms of innate and adaptive immune systems were activated following application of combined formulation. To get a better resolution of the specific immune response profile, we have performed LDA using JMP 15 software. Figure 8 shows canonical plots for the cellular and humoral immune profiles of various treatment groups. It is clearly evident from these plots that combine therapy regimen resulted in strong DC and CD8$^+$ T cell responses (Figure 8A). On the other hand, the rIL15-activated DC group exclusively demonstrated an IL-2 response and the galunisertib + DC group predominantly showed IFN-γ and TNF-α response. Galunisertib-only groups failed to show the above-mentioned cytokine responses (Figure 8B). Although the humoral response of all the treated groups were much stronger compared with that of the PBS group, none of the vaccine groups showed discrimination in Tregs responses, except galunisertib + DC group (Figure 8C). Data further suggest that combined treatment effectively generates strong CD8$^+$ T cell central memory (Figure 8D).

Concurrently, we also assessed the mechanistic and median survival data (mean value for individual immune response) using PCA to identify the correlations between multiple immune parameters and median survival. Median survival was closely correlated with DC and CD8$^+$ T cell responses compared with CD4 responses. It also strongly correlated with IFN-γ and TNF-α cytokine response (Figures 8E and 8F). Correlation between median survival and IFN-γ-producing CD8$^+$ T cells but not CD4$^+$ T cells was strong (Figure 8G). Tregs were negatively correlated with the median survival (Figure 8H). In addition, it was interesting to observe that the median survival correlated well with the central memory (T$_{CM}$) CD8$^+$ T cell response but poorly with the effector memory (T$_{em}$) (Table S2). However, median survival showed a higher correlation with CD8 T cell-derived IFN-γ (correlation coefficient 0.8088) and T$_{cm}$ (correlation coefficient 0.8321) compared with CD8-derived ROS level (correlation coefficient 0.5245) (Table S2). Tumor metastasis and disease progression have a higher correlation coefficient in relation to serum pSMAD2 level (0.8456), serum TGF-β (0.6615), iTreg (0.6833), Treg-derived TGF-β (0.6646), and Nrp-1 (0.7299) (Table S1 and Figures 8I and 8J). Collectively, LDA and PCA revealed that induction of Treg fragility via downregulation of pSMAD2/Neuropilin1 level and Th1 response (IFN-γ) is the best predictor for durable anti-lymphoma immune response in combined therapy with galunisertib and rIL15-activated DC.

DISCUSSION

In the present work, we have introduced a novel therapeutic formulation for therapy against an experimental malignant lymphoma that grows as a semisolid tumor in the peritoneum of AKR/J mice, called DL. For targeting TGF-βRI, various serine/threonine kinase inhibitors, small-molecule inhibitors, have been developed, including LY2157299 monohydrate (Dituri et al., 2013). LY2157299 (galunisertib) is currently in clinical trial for its evaluation with respect to antitumor effects in patients with glioblastoma and hepatocellular carcinoma (Rodon et al., 2013). Studying the tumoricidal activities *in vitro* and *in vivo* remains a challenge for LY2157299. LY2157299 inhibits β1-integrin activation in tumor cells and consequently blocks intravasation of hepatocellular carcinoma cells into the blood vessels (Fransvea et al., 2009; Mazzocca et al., 2009). LY2157299 was in a phase II clinical trial of patients who either failed previous sorafenib treatment or were ineligible to receive sorafenib (NCT01246986, http://clinicaltrials.gov). Patients treated with LY2157299 had remarkable reduction in serum alpha fetoprotein (AFP), plasma TGF-β1, and E-cadherin levels. We have correlated the combined effects of dendritic cells and LY2157299 treatment in DL tumor-bearing mice and its subsequent role with reference to the Tregs and SMAD phosphorylation for therapeutic benefits. CD4$^+$ Tregs are characterized by the expression of a master regulatory transcription factor FOXP3, which constitutes a highly immune-suppressive component of CD4$^+$ T cells for maintaining immune homeostasis (Ferreira et al., 2019; Ohue and Nishikawa, 2019; Wing et al., 2019).
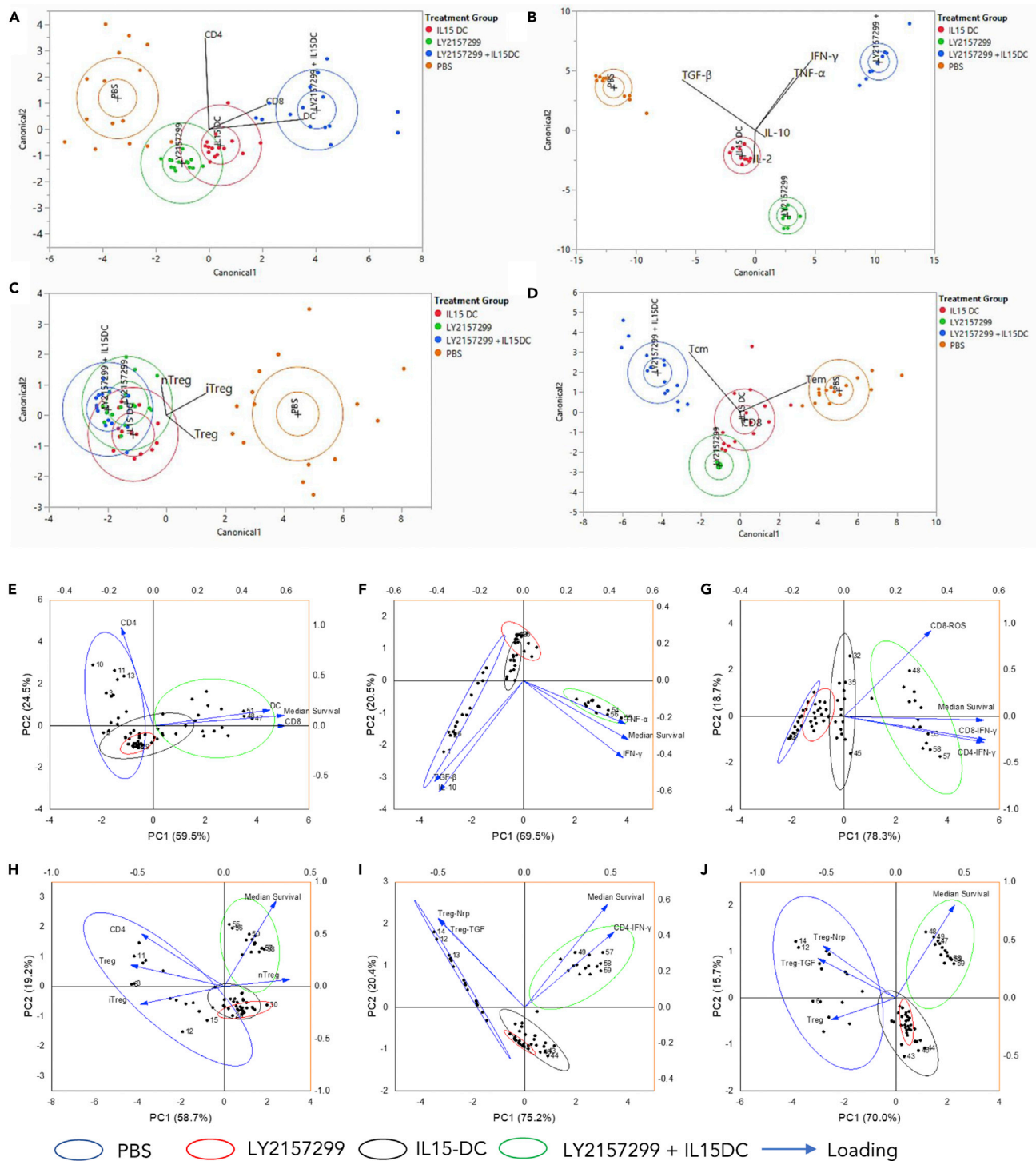
Figure 8. Linear Discriminant and Principal-Component Analyses for Treg Fragility and Th1-Type Humoral Responses as Potential Predictive Biomarkers for Long-Term Immune Protection

(A–J) Various cellular and humoral immune profiles, regulated during the vaccination periods were subjected to analyses by linear discriminant analysis (LDA) and principal-component analysis (PCA) using JMP 15 and Origin Pro 2019 software. Canonical plots showing (A) DC and T cells responses, (B) Th1 & Th2 cytokine response, (C) discriminatory Treg response, and (D) CD8⁺ T cell memory response. Median survival of various treatment groups (Figure 1) and cellular (E & H) and humoral (F, G, I, and J) responses were analyzed by PCA.

Because of their competence and capability to suppress the self-antigen responses, Treg cells may scuttle anti-tumor immune functions. FOXP3^{+} T cells infiltrating into tumor tissues are predominantly FOXP3^{hi} effector Tregs in the majority of neoplastic conditions (Tanaka and Sakaguchi, 2017). High ratio of Treg cells to CD8^{+} T$_c$ cells in tumor sites indicates poor prognosis in various types of cancer (Sato et al., 2005; Tanaka and Sakaguchi, 2017). Thus, targeting Tregs with selective Treg depletion or dysfunction for enhancing tumor-targeted immunity can be of high significance.

In view of the importance and significance of LY2157299 and a possible negative role played by the Tregs in poor prognosis of cancer, we have designed a novel binary therapeutic regimen, including immunotherapy and chemotherapy against a highly aggressive and metastatic lymphoma called DL. This tumor model appears to be very similar to common human B cells lymphomas, which constitute a major category of human cancer worldwide. DL cells are CD3^{−}CD11b^{+}CD19^{+} B cells; they were originally described as sarcoma and later established as a lymphosarcoma in mouse model of oncogenesis (Hira et al., 2014; Klein and Klein, 1954). We have adopted a strategy to combine chemotherapy (LY2157299) with immunotherapy (rIL15-activated DC) against the DL tumor-bearing mice. Our results suggest that the dual therapy significantly enhanced the tumoricidal effects compared with monotherapy either with LY2157299 or cytokine-activated DC. Our results indicate that binary application of LY2157299 + rIL15 DC downregulates the TGF-β, which in turn abrogates the FOXP3 expression in the lymph node as well as in organs like spleen. We emphasized on the effects of the cocktail against lymph node to show how the dual therapy could influence the lymph node architecture, including the expression and distribution of the Tregs.

The neuropilin receptor acts as regulator of nervous system development, via semaphorin co-receptors with plexins. Later, the neuropilins were identified and recognized as receptors for VEGF. Manipulating Nrp-1 and Nrp-2 functions can regulate the tumor cell growth and metastasis through effects on vascular biology and lymphatic biology, respectively (Ferrara and Kerbel, 2005; Pan et al., 2007). A direct role for neuropilins within the tumor cells has also been postulated. Nrp-1 is expressed in widely different types of cancers (i.e., prostate, melanoma, astrocytoma, glioblastoma lung, pancreatic or colon carcinoma, neuroblastoma, leukemia, and lymphoma), suggesting a critical role in tumor progression (Karjalainen et al., 2011; Neufeld and Kessler, 2008; Prud et al., 2012; Yaqoob et al., 2012). A growing number of evidences suggest that Nrp-1 plays important roles independently of contribution from VEGF receptors. Nrp-1 promotes invasiveness in melanoma via activation of selected integrins and by stimulating VEGF-A and metalloproteinases secretion and controlling specific signal transduction pathways in the absence of VEGFR-1/2 (Ruffini et al., 2013). Nrp-1 has close relation with FOXP3^{+} Treg cells and plays the role of a key mediator for Treg cells, infiltrating into the tumor in response to tumor-derived VEGF (Hansen et al., 2012). Numbers of tumor-infiltrating FOXP3^{+} Treg cells were significantly outnumbered, following activation of CD8^{+} T cells within tumors of T cell-specific Nrp-1-deficient mice (Hansen et al., 2012). Treg cells expressed receptor Nrp-1, which interacts both *in vitro*, to potentiate Treg cell functions and survival, and *in vivo*, at inflammatory sites. Treg cell stability and limiting anti-tumor immune responses can be modulated by Sema4a–Nrp-1 axis (Delgoffe et al., 2013). We here addressed the possible role of Nrp-1 in our model of combination therapy against murine lymphoma. Considering the important role played by Nrp-1 and Tregs, we looked into this matter in the context of combination therapy, targeting TGF-βR1 in association with rIL15-activated DC. We have also linked the critical role of SMAD phosphorylation to show how these regulatory pathways might be linked to each other in the pathogenesis of lymphoma. We have tried to explain the correlation of these pathways in the grand landscape of B cell lymphoma using a simple and relevant animal model. Our data showed that dual therapy with galunisertib + rIL15-activated DC becomes significantly tumoricidal and extended the lifespan of the tumor-bearing animals with nearly 75% of the animals surviving for more than 60 days, compared with untreated littermates. This treatment schedule elaborated the expansion of memory CD8^{+} T cell response, accompanied with sharp decline in SMAD2/3 phosphorylation and downregulation of Nrp-1 expression.

TGF-β overexpression is associated with many advanced cancers including lymphomas, and the outcome of its signaling is the development of an immune compromised state that enables tumor progression and metastasis. There is a burgeoning need for additional studies to identify new agents that block TGF-β signaling for therapeutic benefit. Galunisertib or LY2157299 is a pharmacological small molecule inhibitor (a selective ATP-mimetic inhibitor of TGF-β receptor that acts through downregulation of pSAMD2). As a monotherapy, galunisertib has shown some anti-lymphoma activity but with no lasting effects on therapeutic efficacy. Here, we have demonstrated the ability of galunisertib to modulate anti-tumor CD8^{+} T cell

immunity in combination with rIL15-activated DC in a preclinical lymphoma model. Successful binary therapy with rIL15-activated DC was achieved by limiting the Tregs generation with consequent downregulation of FOXP3$^+$CD4$^+$ T$_h$ cells in the TDLN and vascularized organs like spleen. This also associated with the consistent loss pSMAD2 and downregulation of Nrp-1, leading to better prognosis and positive outcome. In the recent past, galunisertib was in clinical trial in combination with checkpoint inhibitors, viz., nivolumab and durvalumab in patients with lung, liver, and pancreatic cancers. However, these attempts were marred with drug intolerance and other complexities. Our data provide a strong justification to explore the potential application of LY2157299 in combination with adoptive transfer of rIL15-activated DC to enhance the anti-lymphoma immune responses.

Limitations of the Study

The present study was aimed to design a comprehensive protocol for binary application of galunisertib and gamma-c cytokine (interleukin-15)-activated dendritic cells against lymphoma. Galunisertib has not been tested either in pre-clinical or in clinical scenarios. The experimental study in mouse model showed significant insight for its possible clinical application. We have traced biochemical and immunological limitations, associated with the exacerbation of the disease, which often leads to metastasis and poor prognosis. However, application of these pre-clinical experimental findings may have number of limitations as each patient is different and so is their disease course. Determination of dose and dose responsive toxicity are critically important parameters to consider. Our animal model study could provide relevant information for possible clinical trial of galunisertib in patients with lymphoma.

Resource Availability

Lead Contact

Further information and requests for resources and reagents should be directed to and will be fulfilled by the Lead Contact, Sumit Kumar Hira (sumit.hira2008@gmail.com).

Materials Availability

This study did not generate new unique reagents.

Data and Code Availability

All data are included in the published article and the Supplemental Information files and any additional information will be available from the lead contact upon request.

METHODS

All methods can be found in the accompanying Transparent Methods supplemental file.

SUPPLEMENTAL INFORMATION

Supplemental Information can be found online at https://doi.org/10.1016/j.isci.2020.101623.

AUTHOR CONTRIBUTIONS

S.K.H., A.R., and A.P. performed the *in vitro* and *in vivo* experiments. A.P., R.S., I.M., and S.K.H. perform the histopathological analysis. S.K.H., A.P., J.S., and S.B. performed the FACS analysis. S.K.H. and P.P.M. conceived, planned, and analyzed the data and wrote the manuscript.

DECLARATION OF INTERESTS

The authors declare that they have no competing interests.

REFERENCES

Akhurst, R.J. (2017). Targeting TGF-β signaling for therapeutic gain. Cold Spring Harb. Perspect. Biol. 9, a022301.

Bhola, N.E., Balko, J.M., Dugger, T.C., Kuba, M.G., Sánchez, V., Sanders, M., Stanford, J., Cook, R.S., and Arteaga, C.L. (2013). TGF-β inhibition enhances chemotherapy action against triple-negative breast cancer. J. Clin. Invest. 123, 1348–1358.

Bueno, L., de Alwis, D.P., Pitou, C., Yingling, J., Lahn, M., Glatt, S., and Trocóniz, I.F. (2008). Semi-mechanistic modelling of the tumour growth inhibitory effects of LY2157299, a new type I receptor TGF-β kinase antagonist, in mice. Eur. J. Cancer 44, 142–150.

Chen, C., Zhao, S., Karnad, A., and Freeman, J.W. (2018). The biology and role of CD44 in cancer progression: therapeutic implications. J. Hematol. Oncol. 11, 64.

Chen, G., Ghosh, P., Osawa, H., Sasaki, C.Y., Rezanka, L., Yang, J., O'Farrell, T.J., and Longo, D.L. (2007). Resistance to TGF-β1 correlates with aberrant expression of TGF-β receptor II in human B-cell lymphoma cell lines. Blood 109, 5301–5307.

Delgoffe, G.M., Woo, S.-R., Turnis, M.E., Gravano, D.M., Guy, C., Overacre, A.E., Bettini, M.L., Vogel, P., Finkelstein, D., Bonnevier, J., et al. (2013). Stability and function of regulatory T cells is maintained by a neuropilin-1–semaphorin-4a axis. Nature 501, 252–256.

Derynck, R., and Budi, E.H. (2019). Specificity, versatility, and control of TGF-β family signaling. Sci. Signal. 12, eaav5183.

Derynck, R., and Zhang, Y.E. (2003). Smad-dependent and Smad-independent pathways in TGF-β family signalling. Nature 425, 577–584.

Dituri, F., Mazzocca, A., Peidrò, F.J., Papappicco, P., Fabregat, I., De Santis, F., Paradiso, A., Sabbà, C., and Giannelli, G. (2013). Differential inhibition of the TGF-β signaling pathway in HCC cells using the small molecule inhibitor LY2157299 and the D10 monoclonal antibody against TGF-β receptor type II. PLoS One 8, e67109.

Ferrara, N., and Kerbel, R.S. (2005). Angiogenesis as a therapeutic target. Nature 438, 967–974.

Ferreira, L.M.R., Muller, Y.D., Bluestone, J.A., and Tang, Q. (2019). Next-generation regulatory T cell therapy. Nat. Rev. Drug Discov. 18, 749–769.

Fransvea, E., Mazzocca, A., Antonaci, S., and Giannelli, G. (2009). Targeting transforming growth factor (TGF)-βRI inhibits activation of β1 integrin and blocks vascular invasion in hepatocellular carcinoma. Hepatology 49, 839–850.

Fujiwara, Y., Nokihara, H., Yamada, Y., Yamamoto, N., Sunami, K., Utsumi, H., Asou, H.,

TakahashI, O., Ogasawara, K., Gueorguieva, I., et al. (2015). Phase 1 study of galunisertib, a TGF-beta receptor I kinase inhibitor, in Japanese patients with advanced solid tumors. Cancer Chemother. Pharmacol. 76, 1143–1152.

Hanahan, D., and Weinberg, Robert A. (2011). Hallmarks of cancer: the next generation. Cell 144, 646–674.

Hansen, W., Hutzler, M., Abel, S., Alter, C., Stockmann, C., Kliche, S., Albert, J., Sparwasser, T., Sakaguchi, S., Westendorf, A.M., et al. (2012). Neuropilin 1 deficiency on CD4+Foxp3+ regulatory T cells impairs mouse melanoma growth. J. Exp. Med. 209, 2001–2016.

Hawke, L.G., Mitchell, B.Z., and Ormiston, M.L. (2020). TGF-β and IL-15 synergize through MAPK pathways to drive the conversion of human NK cells to an innate lymphoid cell 1–like phenotype. J. Immunol. 204, 3171–3181.

Heldin, C.-H., Miyazono, K., and ten Dijke, P. (1997). TGF-β signalling from cell membrane to nucleus through SMAD proteins. Nature 390, 465–471.

Heldin, C.-H., and Moustakas, A. (2012). Role of Smads in TGFβ signaling. Cell Tissue Res. 347, 21–36.

Hill, J.A., Feuerer, M., Tash, K., Haxhinasto, S., Perez, J., Melamed, R., Mathis, D., and Benoist, C. (2007). Foxp3 transcription-factor-dependent and -independent regulation of the regulatory T cell transcriptional signature. Immunity 27, 786–800.

Hira, S.K., Mondal, I., Bhattacharya, D., and Manna, P.P. (2014). Downregulation of endogenous STAT3 augments tumoricidal activity of interleukin 15 activated dendritic cell against lymphoma and leukemia via TRAIL. Exp. Cell Res. 327, 192–208.

Jameson, S.C., and Masopust, D. (2009). Diversity in T cell memory: an embarrassment of riches. Immunity 31, 859–871.

Joseph, J.V., Balasubramaniyan, V., Walenkamp, A., and Kruyt, F.A.E. (2013). TGF-β as a therapeutic target in high grade gliomas – promises and challenges. Biochem. Pharmacol. 85, 478–485.

Karjalainen, K., Jaalouk, D.E., Bueso-Ramos, C.E., Zurita, A.J., Kuniyasu, A., Eckhardt, B.L., Marini, F.C., Lichtiger, B., O'Brien, S., Kantarjian, H.M., et al. (2011). Targeting neuropilin-1 in human leukemia and lymphoma. Blood 117, 920–927.

Klebanoff, C.A., Gattinoni, L., Torabi-Parizi, P., Kerstann, K., Cardones, A.R., Finkelstein, S.E., Palmer, D.C., Antony, P.A., Hwang, S.T., Rosenberg, S.A., et al. (2005). Central memory self/tumor-reactive CD8+ T cells confer superior antitumor immunity compared with effector

memory T cells. Proc. Natl. Acad. Sci. U S A 102, 9571–9576.

Klein, E., and Klein, G. (1954). Differential survival of solid tumor cells after inoculation into established ascites tumors. Cancer Res. 14, 139–144.

Lucas, P.J., Kim, S.-J., Mackall, C.L., Telford, W.G., Chu, Y.-W., Hakim, F.T., and Gress, R.E. (2006). Dysregulation of IL-15-mediated T-cell homeostasis in TGF-beta dominant-negative receptor transgenic mice. Blood 108, 2789–2795.

Massagué, J. (2008). TGFβ in cancer. Cell 134, 215–230.

Massagué, J., Blain, S.W., and Lo, R.S. (2000). TGFβ signaling in growth control, cancer, and heritable disorders. Cell 103, 295–309.

Mazzocca, A., Fransvea, E., Lavezzari, G., Antonaci, S., and Giannelli, G. (2009). Inhibition of transforming growth factor β receptor I kinase blocks hepatocellular carcinoma growth through neo-angiogenesis regulation. Hepatology 50, 1140–1151.

Murthy, V., Katzman, D.P., Tsay, J.-C.J., Bessich, J.L., Michaud, G.C., Rafeq, S., Minehart, J., Mangalick, K., de Lafaille, M.A.C., Goparaju, C., et al. (2019). Tumor-draining lymph nodes demonstrate a suppressive immunophenotype in patients with non-small cell lung cancer assessed by endobronchial ultrasound-guided transbronchial needle aspiration: a pilot study. Lung Cancer 137, 94–99.

Neufeld, G., and Kessler, O. (2008). The semaphorins: versatile regulators of tumour progression and tumour angiogenesis. Nat. Rev. Cancer 8, 632–645.

Neuzillet, C., Tijeras-Raballand, A., Cohen, R., Cros, J., Faivre, S., Raymond, E., and de Gramont, A. (2015). Targeting the TGFβ pathway for cancer therapy. Pharmacol. Ther. 147, 22–31.

Ohue, Y., and Nishikawa, H. (2019). Regulatory T (Treg) cells in cancer: can Treg cells be a new therapeutic target? Cancer Sci. 110, 2080–2089.

Padua, D., and Massagué, J. (2009). Roles of TGFβ in metastasis. Cell Res. 19, 89–102.

Pan, Q., Chanthery, Y., Liang, W.-C., Stawicki, S., Mak, J., Rathore, N., Tong, R.K., Kowalski, J., Yee, S.F., Pacheco, G., et al. (2007). Blocking neuropilin-1 function has an additive effect with anti-VEGF to inhibit tumor growth. Cancer Cell 11, 53–67.

Ponta, H., Sherman, L., and Herrlich, P.A. (2003). CD44: from adhesion molecules to signalling regulators. Nat. Rev. Mol. Cell Biol. 4, 33–45.

Prud, Homme, G.J., and Glinka, Y. (2012). Neuropilins are multifunctional coreceptors

involved in tumor initiation, growth, metastasis and immunity. Oncotarget 3, 921–939.

Roberts, A.B., Anzano, M.A., Lamb, L.C., Smith, J.M., and Sporn, M.B. (1981). New class of transforming growth factors potentiated by epidermal growth factor: isolation from non-neoplastic tissues. Proc. Natl. Acad. Sci. U S A 78, 5339–5343.

Rodón, J., Carducci, M., Sepulveda-Sánchez, J.M., Azaro, A., Calvo, E., Seoane, J., Braña, I., Sicart, E., Gueorguieva, I., Cleverly, A., et al. (2015). Pharmacokinetic, pharmacodynamic and biomarker evaluation of transforming growth factor-β receptor I kinase inhibitor, galunisertib, in phase 1 study in patients with advanced cancer. Invest. New Drugs 33, 357–370.

Rodon, J., Carducci, M.A., Sepúlveda, J.M., Azaro, A., Calvo, E., Seoane, J., Brana, I., Sicart, E., Gueorguieva, I., Cleverly, A., et al. (2013). Integrated data review of the first-in-human dose (FHD) study evaluating safety, pharmacokinetics (PK), and pharmacodynamics (PD) of the oral transforming growth factor-beta (TGF-β) receptor I kinase inhibitor, LY2157299 monohydrate (LY). J. Clin. Oncol. 31, 2016.

Rotman, J., Koster, B.D., Jordanova, E.S., Heeren, A.M., and de Gruijl, T.D. (2019). Unlocking the therapeutic potential of primary tumor-draining lymph nodes. Cancer Immunol. Immunother. 68, 1681–1688.

Ruffini, F., D'Atri, S., and Lacal, P.M. (2013). Neuropilin-1 expression promotes invasiveness of melanoma cells through vascular endothelial growth factor receptor-2-dependent and -independent mechanisms. Int. J. Oncol. 43, 297–306.

Sallusto, F., Geginat, J., and Lanzavecchia, A. (2004). Central memory and effector memory T cell subsets: function, generation, and maintenance. Annu. Rev. Immunol. 22, 745–763.

Sallusto, F., Lenig, D., Förster, R., Lipp, M., and Lanzavecchia, A. (1999). Two subsets of memory T lymphocytes with distinct homing potentials and effector functions. Nature 401, 708–712.

Sanjabi, S., Mosaheb, M.M., and Flavell, R.A. (2009). Opposing effects of TGF-beta and IL-15 cytokines control the number of short-lived effector CD8+ T cells. Immunity 31, 131–144.

Sarris, M., Andersen, K.G., Randow, F., Mayr, L., and Betz, A.G. (2008). Neuropilin-1 expression on regulatory T cells enhances their interactions with dendritic cells during antigen recognition. Immunity 28, 402–413.

Sato, E., Olson, S.H., Ahn, J., Bundy, B., Nishikawa, H., Qian, F., Jungbluth, A.A., Frosina, D., Gnjatic, S., Ambrosone, C., et al. (2005). Intraepithelial CD8+ tumor-infiltrating lymphocytes and a high CD8+/regulatory T cell ratio are associated with favorable prognosis in ovarian cancer. Proc. Natl. Acad. Sci. U S A 102, 18538–18543.

Serova, M., Tijeras-Raballand, A., Dos Santos, C., Albuquerque, M., Paradis, V., Neuzillet, C., Benhadji, K.A., Raymond, E., Faivre, S., and de Gramont, A. (2015). Effects of TGF-beta signalling inhibition with galunisertib (LY2157299) in hepatocellular carcinoma models and in ex vivo whole tumor tissue samples from patients. Oncotarget 6, 21614–21627.

Suzuki, K., Kumanogoh, A., and Kikutani, H. (2008). Semaphorins and their receptors in immune cell interactions. Nat. Immunol. 9, 17–23.

Tanaka, A., and Sakaguchi, S. (2017). Regulatory T cells in cancer immunotherapy. Cell Res. 27, 109–118.

Trotta, R., Dal Col, J., Yu, J., Ciarlariello, D., Thomas, B., Zhang, X., Allard, J., 2nd, Wei, M., Mao, H., Byrd, J.C., et al. (2008). TGF-beta utilizes SMAD3 to inhibit CD16-mediated IFN-gamma production and antibody-dependent cellular cytotoxicity in human NK cells. J. Immunol. 181, 3784–3792.

von Andrian, U.H., and Mackay, C.R. (2000). T-cell function and migration — two sides of the same coin. N. Engl. J. Med. 343, 1020–1034.

Wing, J.B., Tanaka, A., and Sakaguchi, S. (2019). Human FOXP3+ regulatory T cell heterogeneity and function in autoimmunity and cancer. Immunity 50, 302–316.

Yang, L., and Moses, H.L. (2008). Transforming growth factor beta: tumor suppressor or promoter? Are host immune cells the answer? Cancer Res. 68, 9107–9111.

Yang, Z.-Z., Grote, D.M., Ziesmer, S.C., Xiu, B., Yates, N.R., Secreto, F.J., Hodge, L.S., Witzig, T.E., Novak, A.J., and Ansell, S.M. (2013). Soluble and membrane-bound TGF-β-mediated regulation of intratumoral T cell differentiation and function in B-cell non-hodgkin lymphoma. PLoS One 8, e59456.

Yaqoob, U., Cao, S., Shergill, U., Jagavelu, K., Geng, Z., Yin, M., de Assuncao, T.M., Cao, Y., Szabolcs, A., Thorgeirsson, S., et al. (2012). Neuropilin-1 stimulates tumor growth by increasing fibronectin fibril assembly in the tumor microenvironment. Cancer Res. 72, 4047–4059.

Yu, J., Wei, M., Becknell, B., Trotta, R., Liu, S., Boyd, Z., Jaung, M.S., Blaser, B.W., Sun, J., Benson, D.M., et al. (2006). Pro- and antiinflammatory cytokine signaling: reciprocal antagonism regulates interferon-gamma production by human natural killer cells. Immunity 24, 575–590.

Zöller, M. (2011). CD44: can a cancer-initiating cell profit from an abundantly expressed molecule? Nat. Rev. Cancer 11, 254–267.

Supplemental Information

Galunisertib Drives Treg Fragility

and Promotes Dendritic Cell-Mediated

Immunity against Experimental Lymphoma

Sumit Kumar Hira, Abhinandan Rej, Ankush Paladhi, Ranjeet Singh, Jayasree Saha, Indrani Mondal, Sankar Bhattacharyya, and Partha Pratim Manna
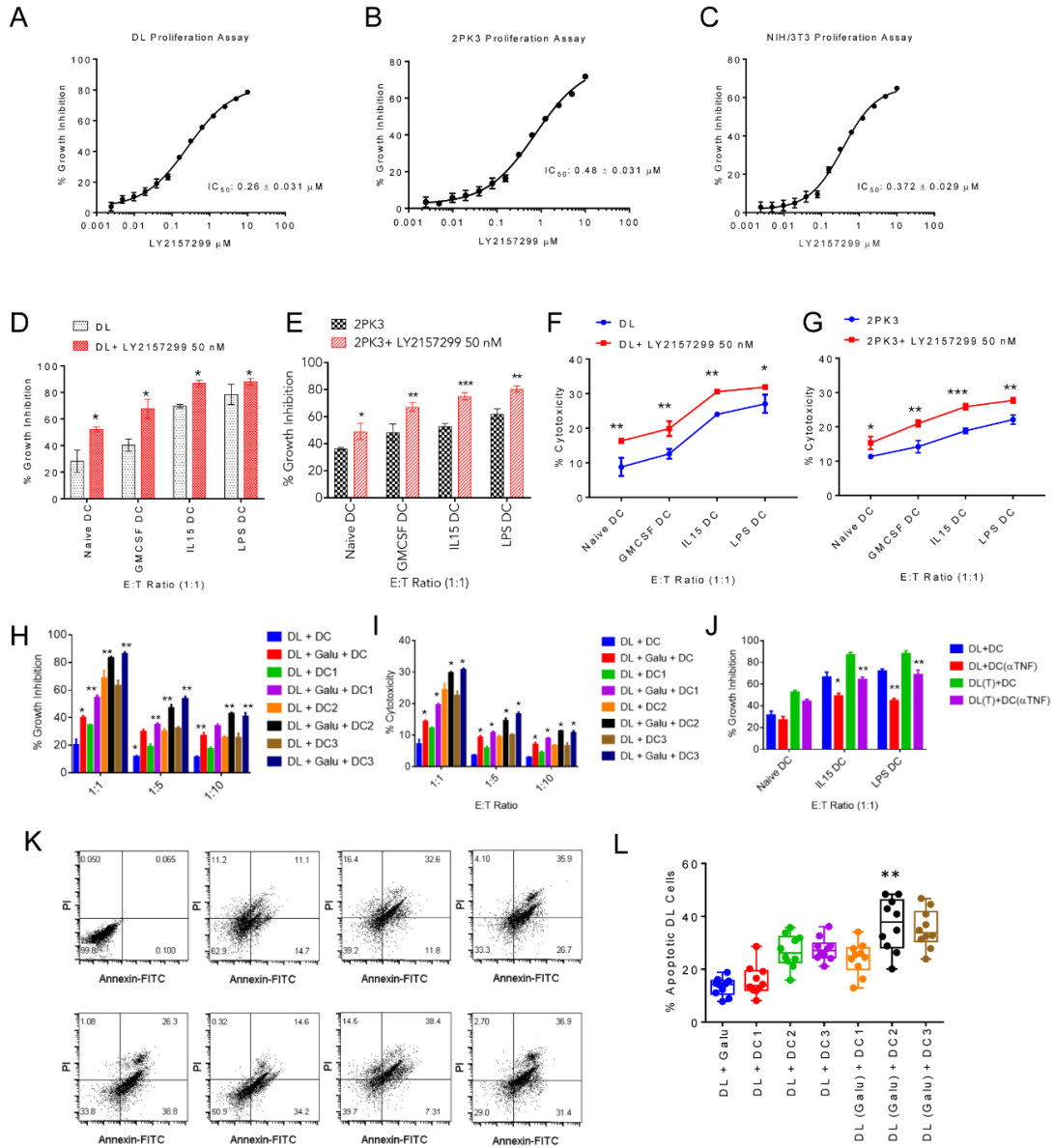
Figure S1 Related to Figure 1

Fig. S 1 In vitro tumoricidal activity of Galunisertib only or in combination with IL-15DC. (A-C) Growth inhibition DL, 2PK3 and NIH/3T3 cell in the presence of increasing concentration of LY257299 (Galunisertib). (D & E) Enhancement of growth inhibition of LY257299 treated DL and 2PK3 cells by GMCSF (1000 U/ml) and IL-15 (200 pg/ml) activated DC. LPS (10 µg/ml) acts as a positive control. (F & G) Direct cytotoxicity of cytokine activated DC against DL and 2PK3 cells. (H & I) Growth inhibition of DL and 2PK3 cells in the presence of cytokine activated DC in reverse E:T ratios. (J) Ablation of cytokine activated DC mediated growth inhibition of DL tumor cells in the presence of neutralizing anti TNF-α at an E:T ratio 1:1. (K & L) Annexin V staining for the assessment of percent apoptosis in DL tumor cells in the presence of cytokine activated DC. FSC/SSC was used to discriminate the tumor cells from the DC for assessment of Annexin positivity. Data are presented as mean±SD, n=5, Two-way ANOVA, Holm-Sidak Post-hoc test *$p<0.05$, ** $p<0.01$, *** $p<0.001$.
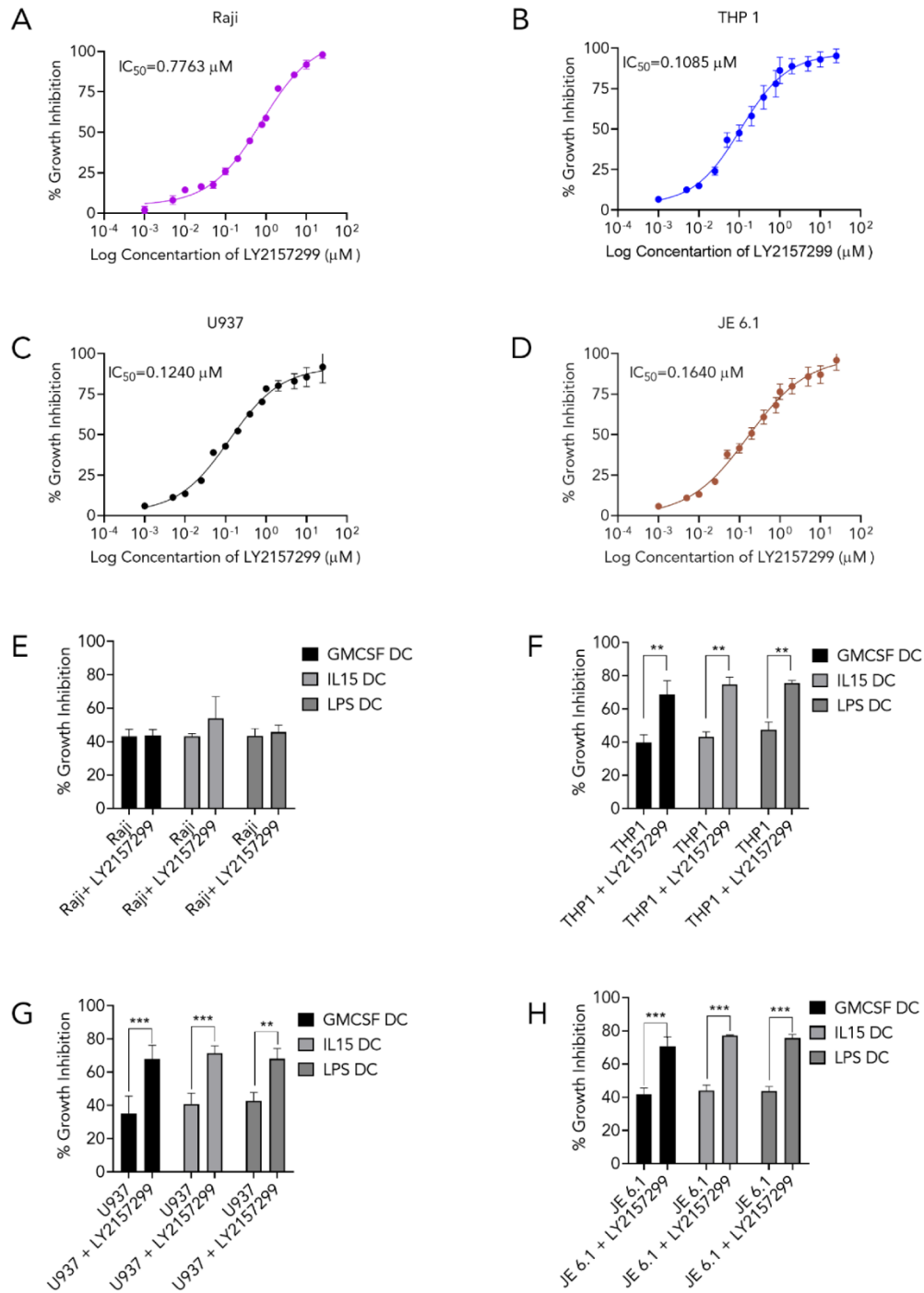
Figure S2 Related to Figure 1

Fig. S 2 In vitro tumoricidal activity of LY2157299 and LY2157299+DC against Raji, THP-1, U937 and JE6.1 cells. (A-D) Concentration dependent growth inhibition of Raji, THP-1, U937 and JE6.1 in the presence of LY2157299, assessed by 48 hours MTT assay. (E-H) Assessment of growth inhibition of Raji, THP-1, U937 and JE6.1 cells in the presence or absence of naive DC (GMCSF DC) or activated DC (IL-15 DC & LPS DC) and LY2157299 by 48 hours MTT assay. Data presented as Mean ± SD of triplicate determination in each case. Two-way ANOVA, Holm-Sidak Post-hoc test *$p<0.05$, ** $p<0.01$, *** $p<0.001$.
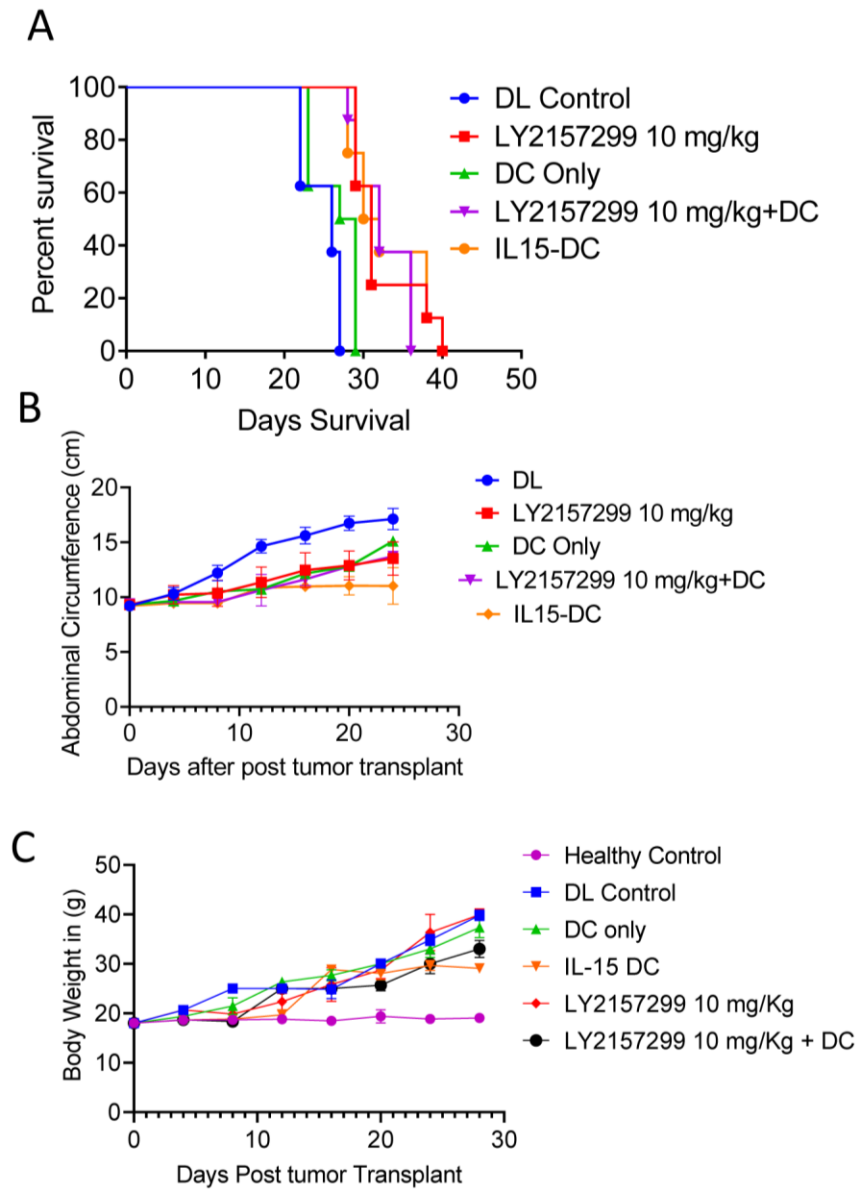
Figure S3 Related to Figure 1

Fig. S 3 *Naive DC has negligible antitumor potential against established DL lymphoma.*

DL tumor bearing mice were either treated with naive DC or LY2157299 only or in indicated combination as described in materials and methods. (A) Kaplan-Meier survival analysis of the animals received the indicated treatment. (B) Measurement of abdominal circumferences (tumor volume) in mice received the indicated treatment. (C) Body weight of the untreated and treated groups for the indicated time period. Data presented as (Mean ± SD, n=8), from summary of data of five different mice from each group.
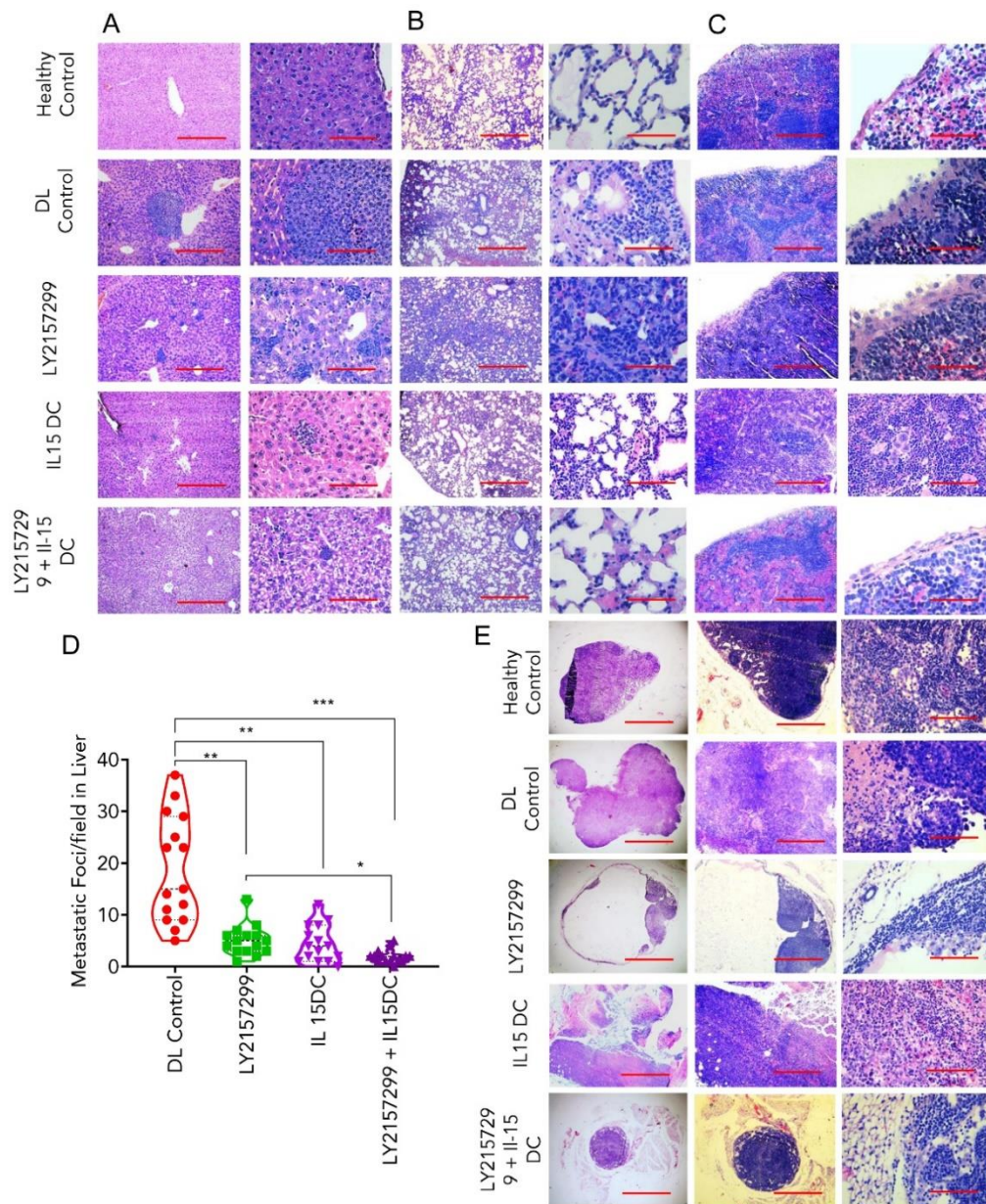
Figure S4 Related to Figure 1

Fig. S 4. Histopathological analysis of tumor invasion and ablation in untreated and dual therapy treated DL tumor bearing mice. (A-C) Histopathological analysis of liver (A), lung (B) and spleen (C) of DL untreated (ii), LY2157299 only (iii) or LY2157299+IL-15DC (iv) treated mice compared with healthy control (i) magnification 100× and 400×. (D) Quantification of metastatic foci in the liver of untreated or treated groups. Data represents Mean±SD of at least 10 animals (n=3) per group. (E) Lymph node architecture in untreated DL (ii) and DL mice treated with either LY2157299 only (iii) or LY2157299+IL-15DC (iv) was analysed by histopathological section of the affected nodes. Nodes from healthy control (i) was used a s reference control for comparison. The architecture of tumor draining lymph nodes (ii) from mice with fully developed disease where infiltration of tumor cells (blue arrow) and tumor necrosis was (red circle) observed. (iii) & (iv) therapy recruited macrophage/DC (cells with foamy cytoplasm, indicated with red arrow) on Tumor-Draining Lymph and clear the infiltrated tumor cells in TDLN. In combined treatment (iv) reduced the adjacent LN (arrow) medullary hyperplasia (40×, 100× and 400× magnification). Scale bar = 50 μm.

Figure S5 Related to Figure 2
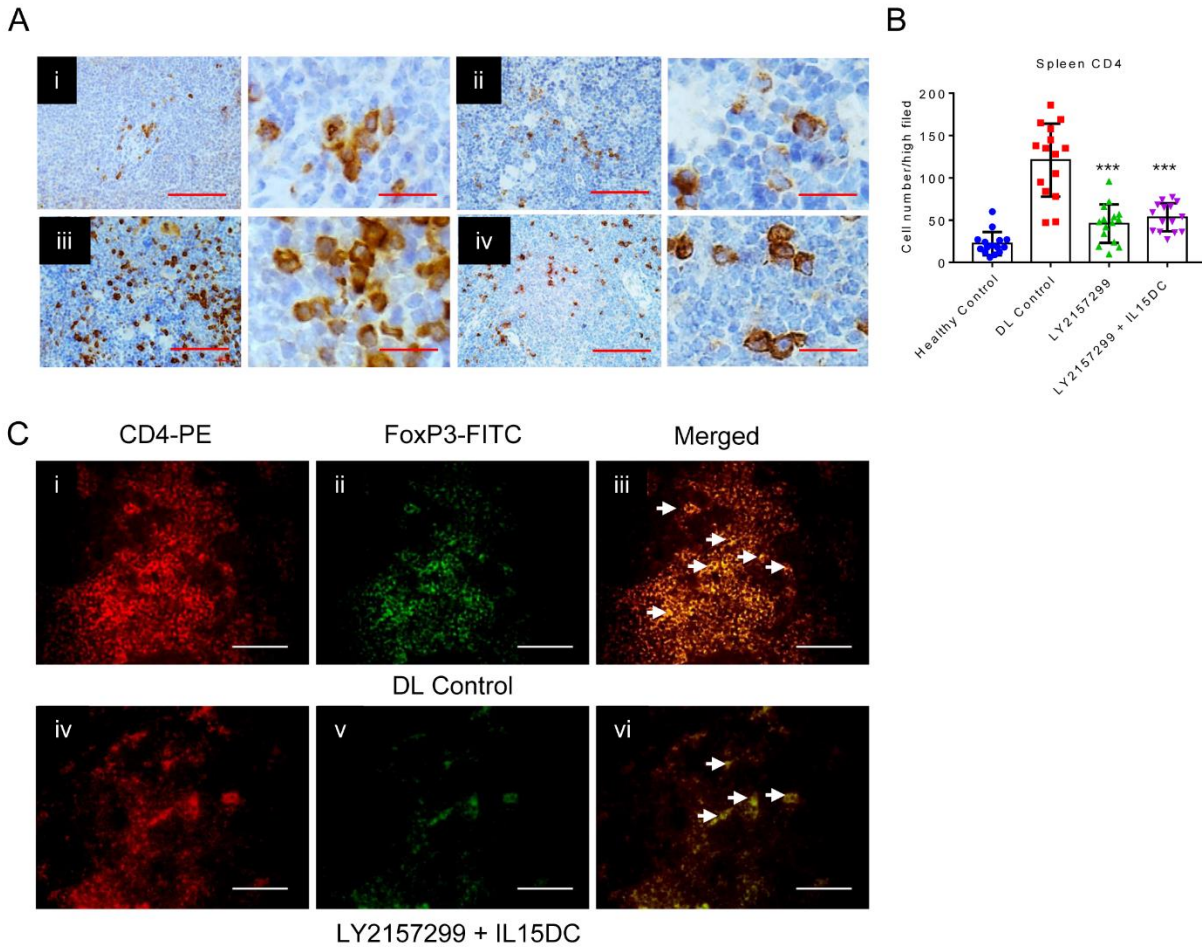
Fig. S 5 Distribution of FOXP3+ T cells in splenic architecture before and after the dual therapy in tumor bearing mice. (A) Immunohistochemical staining of FOXP3+ cells in spleen of untreated DL (ii) and DL mice treated either with LY2157299 only (iii) or LY2157299+IL-15DC (iv). Healthy control spleen was used as control (i)magnification 100× and 400×. Scale bar = 50 µm. (B) Quantification of FOXP3+ cells in spleen following above treatment in A. (C) Paraffin sections of spleens were stained with anti-mouse CD4-PE mAb (red) and anti-mouse FOXP3-FITC (green) and analyzed using DMi8 fluorescence microscope, magnification 400×. Reduced expression of FOXP3 in LY2157299+IL-15DC spleen with a smaller number of co-localizations as indicated by the arrows (white). Data are presented as mean±SD, n=4, Two-way ANOVA, Holm-Sidak Post-hoc test *** p<0.001.

Figure S6 Related to Figure 7
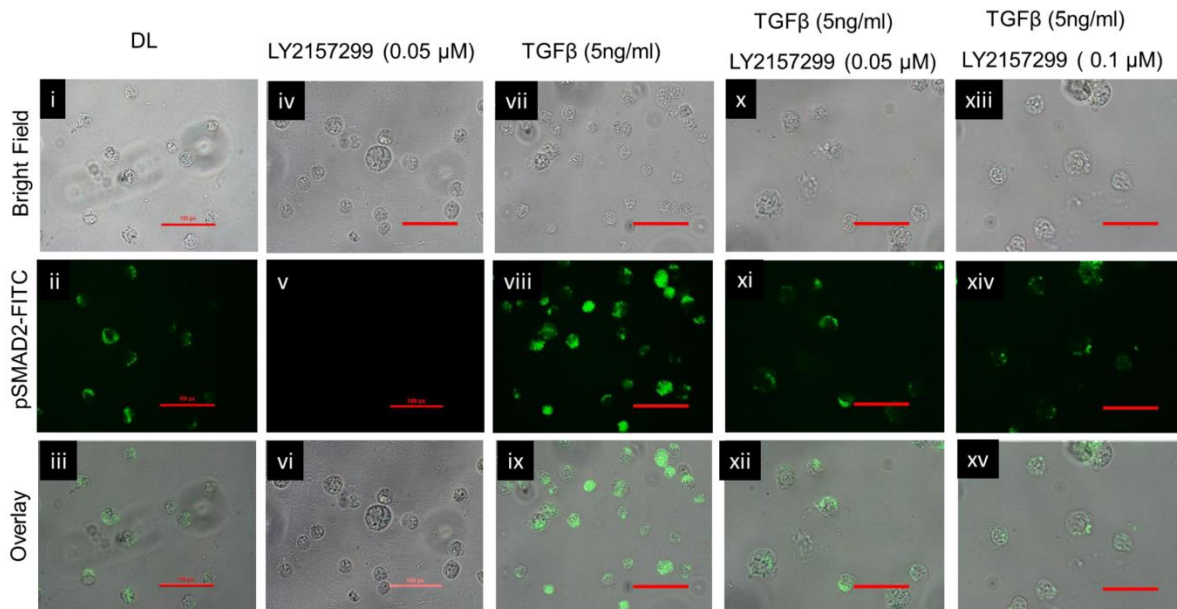
Fig. S 6 Demonstration of SMAD phosphorylation in DL tumor cells treated with TGF-ϐ and increasing concentration of Galunisertib. DL tumor cells were treated with TGF-β (5 ng/ml) for 5 hrs followed by treatment with increasing concentrations of LY2157299 at 37°C, 5% CO_2. The cells were washed in PBS (×2) and stained with FITC-labelled anti pSMAD2 antibody for 2h and was observed under microscope (Nikon 80i). Representative image of 3 similar experiments is shown. Scale bar = 50 μm.

Figure S7 Related to Figure 7
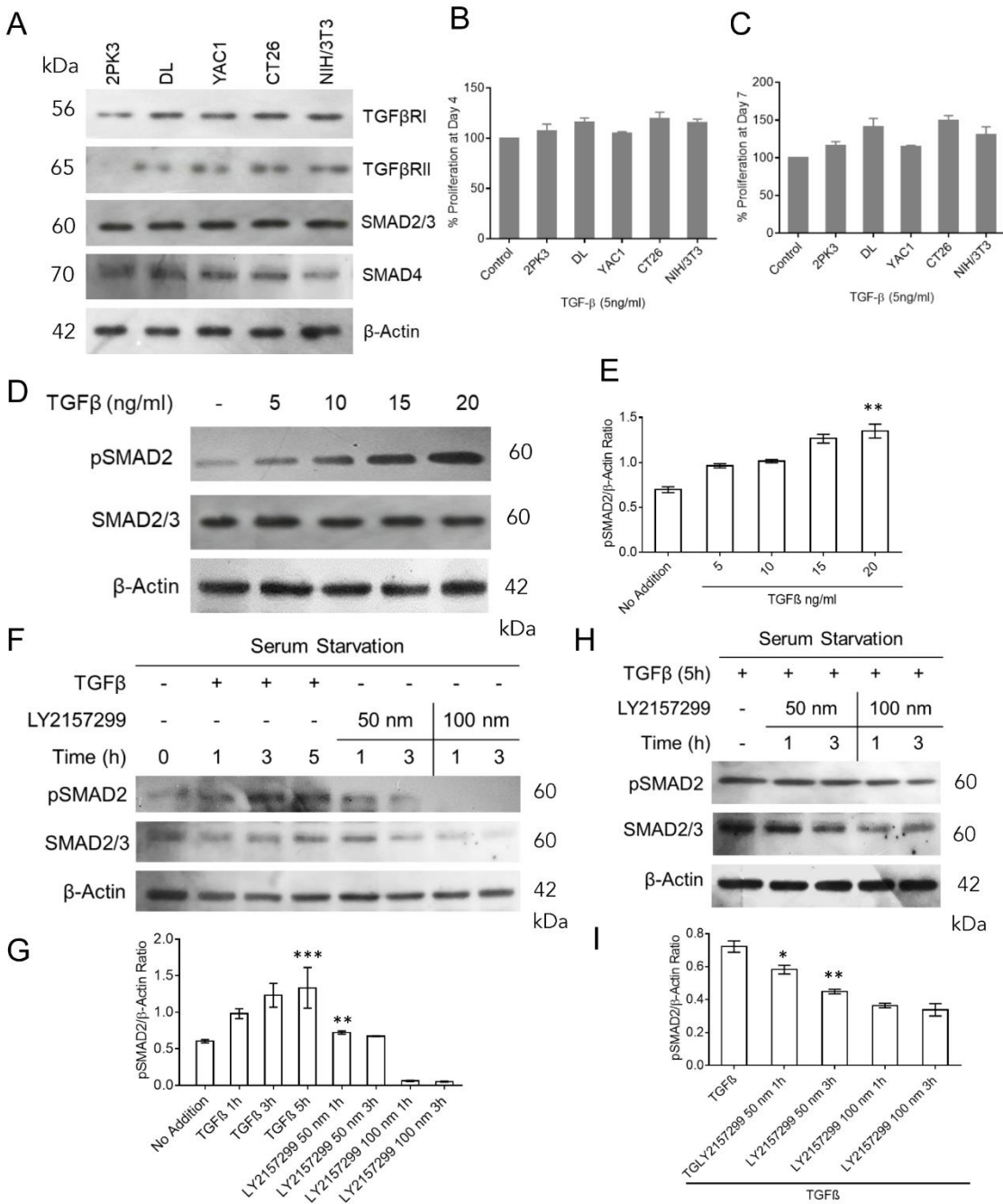
Fig. S 7 DL tumor cells show SMAD phosphorylation in TGF-ß responsive manner. (A) Protein levels of TGF-βR1, TGF-βR2, SMAD2/3, and SMAD4 by Western blotting in a panel of TGF-β responsive cell lines (2PK3, YAC1, CT26, and NIH/3T3) and DL cells. (B & C) Proliferation of DL, 2PK3, YAC1, CT26, and NIH/3T3 cells in the presence of TGF-β (5 ng/mL) for 4 and 7 days. (D & E) Effects of TGF-β on the levels of pSMAD2 expression in DL cells as assessed by Western blotting and Densitometric analysis. (F-I) SMAD phosphorylation was evaluated by Western blotting in DL tumor cells following treatment with LY2157299 with or without TGF-β stimulation in serum free condition. Data presented as Mean ± SD of triplicate determination in each case. Two-way ANOVA, Holm-Sidak Post-hoc test *p<0.05, ** p<0.01, *** p<0.001.

Figure S8 Related to Figure 4
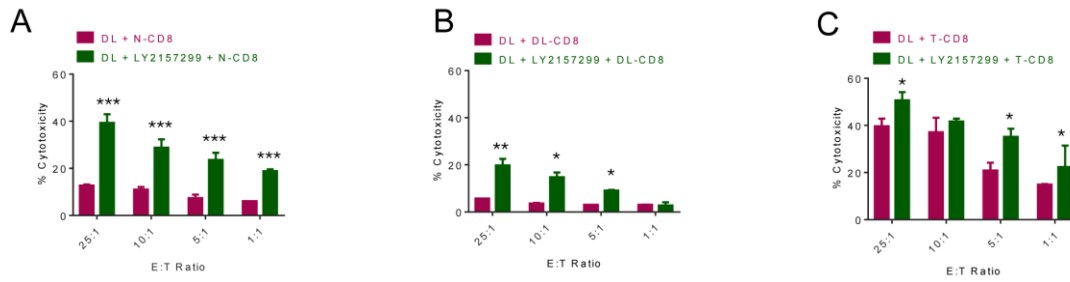
Fig. S 8 CD8+ T cells derived from mice with dual therapy have potent cytotoxicity against the DL target cells. (A-C) Enhanced antigen specific cytotoxicity of CD8^{+} T cells derived from the LY2157299+IL-15DC treated mice and compared with untreated DL mice. DL mice treated with LY2157299 only show intermediate but enhanced CD8+ T cytotoxicity compared to untreated condition. Data presented as Mean ± SD of triplicate determination in each case. Representative of one experiment out of three performed is shown. Two-way ANOVA, Holm-Sidak Post-hoc test *p<0.05, ** p<0.01, *** p<0.001.

Figure S9 Related to Figure 1
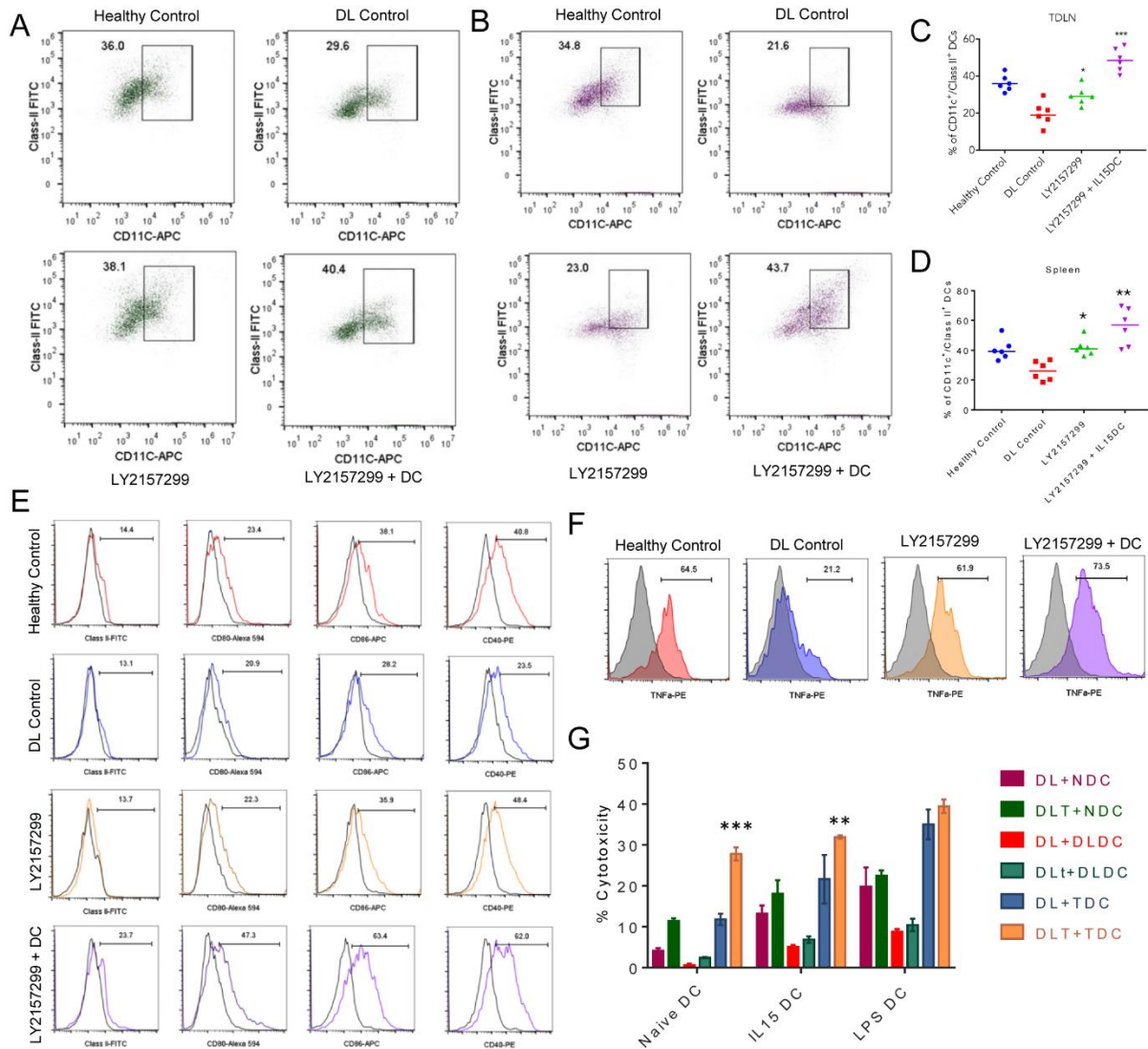
Fig. S9 Galunisertib+IL-15DC treatment corrects the impaired immune functions of DC and boost cytotoxicity and TNF-α production. (A &C) FACS analysis and quantification of infiltrated CD11c+/Class II DC in lymph node and in (B & D) spleen of untreated DL or DL mice with indicated treatment. DC from healthy animals was used as control. (E) Restoration of Class II and co-stimulatory molecules (CD40, CD80 and CD86) in LY2157299+IL-15DC treated animals compare with untreated DL mice. Representative of one experiment out of three performed is shown. (F) Enhanced expression of TNF-α (% positive cells) in DC, derived from the surviving vaccinated mice. (G) Restoration of impaired DC cytotoxicity in mice treated with LY2157299+IL-15DC against DL and DL cell pre-treated with suboptimal concentration of LY2157299. Data presented as Mean ± SD of triplicate determination in each case. Two-way ANOVA, Holm-Sidak Post-hoc test *p<0.05, ** p<0.01, *** p<0.001.

Figure S10 Related to Figure 1
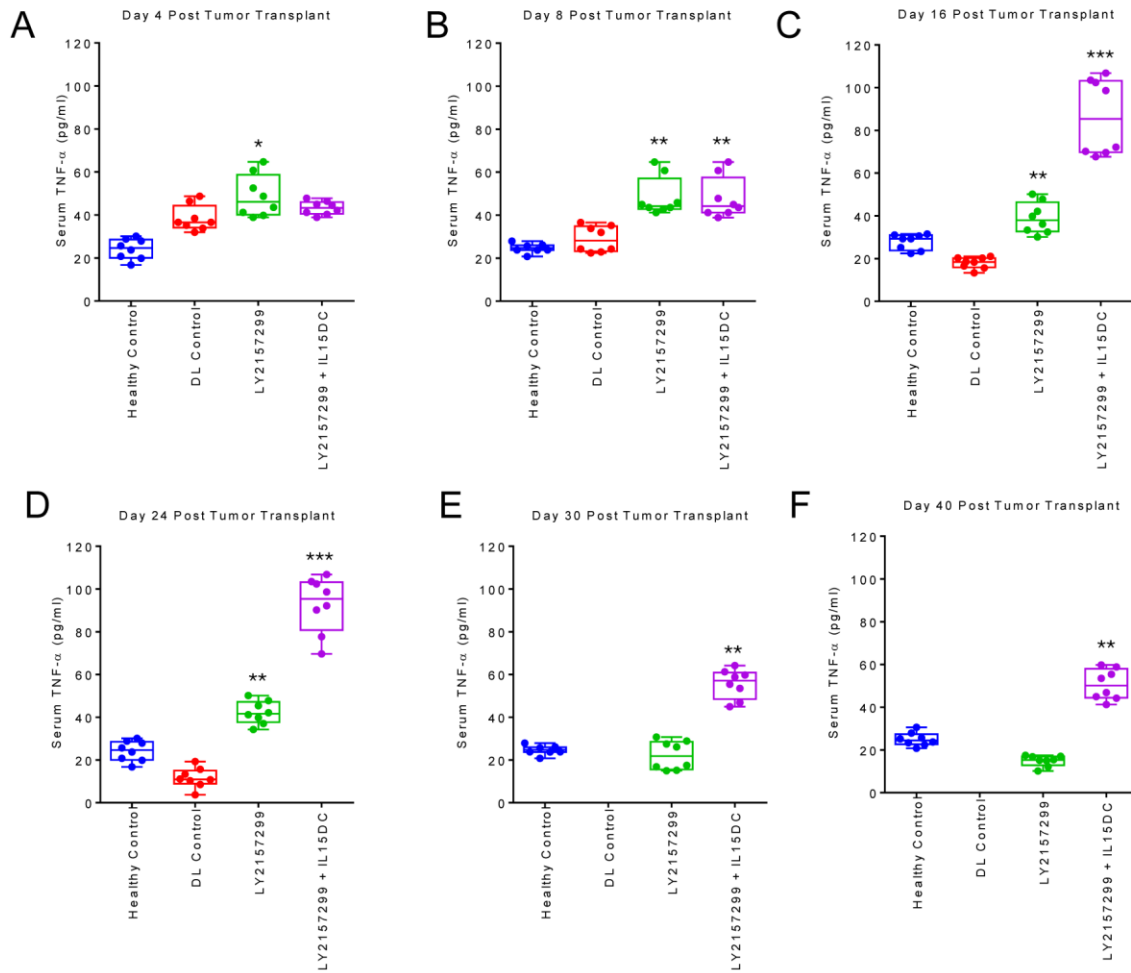
Fig. S10 Elevated TNF-α generation in Galunisertib+IL-15DC treated animals demonstrated positive immune regulation. (A-F) Serum TNF-α level in mice treated with LY2157299+IL-15DC compared to untreated DL mice at day 4, 8, 16, 32 and 40. Data represent Mean ± SD of 7 mice of 3 independent experiments. Two-way ANOVA, Holm-Sidak Post-hoc test *p<0.05, ** p<0.01, *** p<0.001.

Figure S11 Related to Figure 2
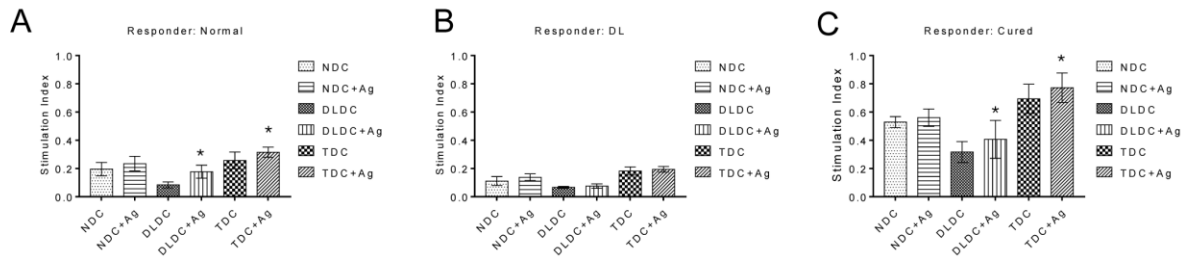
Fig. S 11 Antigen specific CD4+T cell proliferation in mice treated with Galunisertib+IL-15 DC. (A-C)
Antigen specific proliferation of CD4+T cells derived from the animals treated with LY2157299+IL-15DC
and compared with untreated DL mice. DL mice treated with LY2157299 alone show intermediate but
enhanced CD4+ T cell proliferation compared to untreated condition. Data presented as Mean ± SD of
triplicate determination in each case. Representative of one experiment out of three performed is shown.
Two-way ANOVA, Holm-Sidak Post-hoc test *p<0.05.

Supplementary Table S1 Abdominal Circumference, Related to Figure 1

Table S1A

Days	DL	LY2157299		
		10mg/kg	50mg/kg	75mg/kg
0				
4	10.30 ± 0.59	10.24 ± 0.78	10.48 ± 0.78	9.50 ± 0.96
8	12.20 ± 0.71	10.71 ± 0.87	10.47 ± 1.22	10.71 ± 0.87
12	14.6445 ± 0.61	12.39 ± 1.1	11.74 ± 1.72	10.49 ± 1.72
16	15.6195 ± 0.76	13.69 ± 0.94	13.07 ± 1.40	10.79 ± 1.64
20	16.74075 ± 0.65	14.98 ± 0.92	14.01 ± 1.87	11.69 ± 1.78
24	17.13075 ± 0.97	17.98 ± 1.30	14.28 ± 1.68	13.89 ± 1.48

Table S1B

Days	DL	DC only	LY2157299	IL15DC Only	LY2157299 + DC	LY2157299 + IL15 DC
0	9.2 ± 0.068	9.3 ± 0.025	9.3 ± 0.045	9.2 ± 0.18	9.4 ± 0.28	9.2 ± 0.048
4	10.30 ± 0.59	9.66 ± 0.15	10.23 ± 0.84	9.46 ± 0.23	9.56 ± 0.32	9.73 ± 0.50
8	12.20 ± 0.71	10.52 ±0.47	10.35 ± 1.19	9.46 ± 0.23	9.56 ± 0.32	9.85 ± 0.71
12	14.64 ± 0.61	10.73 ± 0.41	11.36 ± 1.38	10.86 ± 0.15	10.64 ± 1.43	10.49 ± 0.97
16	15.61 ± 0.76	12.16 ± 0.32	12.45 ± 1.59	10.98 ± 0.20	11.63 ± 0.55	11.45 ± 1.60
20	16.74 ± 0.65	12.8 ± 0.3	12.89 ± 1.32	11.04 ± 0.83	12.8 ± 0.3	10.52 ± 0.47
24	17.13 ± 0.97	15.1 ± 0.26	13.53 ± 1.52	11.03 ± 1.67	13.73 ±0.20	9.65 ± 0.51

Supplementary Table S2: Correlation coefficient matrix of potential predictive biomarkers for long-term immune protection, Related to Figure 8

	Median Survival	CD4	CD8	DC	T_{reg}	iT_{reg}	nT_{reg}	T_{reg}-Nrp-1	T_{reg}-TGF-β	IFN-γ	TNF-α	IL-10	CD8-IFN-γ	CD4-IFN-γ	CD8-ROS	T_{cm}	T_{em}	Metastasis	pSMAD2	TGF-β
Median Survival	1.0000	-0.0987	0.8059	0.6052	-0.4810	-0.4652	0.2608	-0.4781	-0.5095	0.9131	0.8166	-0.4731	0.8088	0.7818	0.5245	0.8321	-0.4568	-0.4808	-0.4536	-0.7620
CD4	-0.0987	1.0000	-0.1816	-0.0665	0.3509	0.5513	-0.3905	0.5313	0.6103	0.0035	-0.1086	0.5034	-0.1845	-0.2031	-0.1556	0.0674	0.6656	0.8219	0.7431	0.3687
CD8	0.8059	-0.1816	1.0000	0.6039	-0.4634	-0.4972	0.2481	-0.4513	-0.5219	0.8301	0.6769	-0.4433	0.7968	0.7768	0.6180	0.7955	-0.4110	-0.5050	-0.4597	-0.7246
DC	0.6052	-0.0665	0.6039	1.0000	-0.4882	-0.3560	0.0144	-0.1361	-0.3849	0.6165	0.5434	-0.4772	0.4489	0.4143	0.7450	0.7577	-0.2635	-0.3599	-0.3148	-0.4455
T_{reg}	-0.4810	0.3509	-0.4634	-0.4882	1.0000	0.5994	-0.4050	0.4988	0.6767	-0.4182	-0.4861	0.8773	-0.4992	-0.5024	-0.4209	-0.3184	0.6506	0.4513	0.6510	0.7402
iT_{reg}	-0.4652	0.5513	-0.4972	-0.3560	0.5994	1.0000	-0.4475	0.7708	0.8895	-0.3776	-0.5344	0.5938	-0.5409	-0.5573	-0.5497	-0.3039	0.7586	0.6833	0.7040	0.6785
nT_{reg}	0.2608	-0.3905	0.2481	0.0144	-0.4050	-0.4475	1.0000	-0.4147	-0.4110	0.2547	0.2718	-0.5354	0.3502	0.3733	0.1175	0.0309	-0.4986	-0.3783	-0.4556	-0.4840
T_{reg}-Nrp-1	-0.4781	0.5313	-0.4513	-0.1361	0.4988	0.7708	-0.4147	1.0000	0.9064	-0.3547	-0.5343	0.5362	-0.6223	-0.6462	-0.2243	-0.2014	0.7960	0.6646	0.6199	0.6505
T_{reg}-TGF-β	-0.5095	0.6103	-0.5219	-0.3849	0.6767	0.8895	-0.4110	0.9064	1.0000	-0.4118	-0.5655	0.6980	-0.5902	-0.6038	-0.4123	-0.3053	0.8787	0.7299	0.7388	0.7013
IFN-γ	0.9131	0.0035	0.8301	0.6165	-0.4182	-0.3776	0.2547	-0.3547	-0.4118	1.0000	0.7842	-0.3910	0.8666	0.8317	0.5197	0.8667	-0.3620	-0.4121	-0.3597	-0.6948
TNF-α	0.8166	-0.1086	0.6769	0.5434	-0.4861	-0.5344	0.2718	-0.5343	-0.5655	0.7842	1.0000	-0.4723	0.8154	0.8015	0.5313	0.7048	-0.4970	-0.5131	-0.4968	-0.7525
IL-10	-0.4731	0.5034	-0.4433	-0.4772	0.8773	0.5938	-0.5354	0.5362	0.6980	-0.3910	-0.4723	1.0000	-0.4929	-0.5030	-0.4216	-0.2810	0.6722	0.5867	0.6962	0.7492
CD8-IFN-γ	0.8088	-0.1845	0.7968	0.4489	-0.4992	-0.5409	0.3502	-0.6223	-0.5902	0.8666	0.8154	-0.4929	1.0000	0.9967	0.4082	0.7143	-0.4669	-0.5475	-0.5056	-0.8562
CD4-IFN-γ	0.7818	-0.2031	0.7768	0.4143	-0.5024	-0.5573	0.3733	-0.6462	-0.6038	0.8317	0.8015	-0.5030	0.9967	1.0000	0.3861	0.6775	-0.4663	-0.5546	-0.5154	-0.8679
CD8-ROS	0.5245	-0.1556	0.6180	0.7450	-0.4209	-0.5497	0.1175	-0.2243	-0.4123	0.5197	0.5313	-0.4216	0.4082	0.3861	1.0000	0.6877	-0.3131	-0.4752	-0.4408	-0.5233
T_{cm}	0.8321	0.0674	0.7955	0.7577	-0.3184	-0.3039	0.0309	-0.2014	-0.3053	0.8667	0.7048	-0.2810	0.7143	0.6775	0.6877	1.0000	-0.1695	-0.3777	-0.2816	-0.5763
T_{em}	-0.4568	0.6656	-0.4110	-0.2635	0.6506	0.7586	-0.4986	0.7960	0.8787	-0.3620	-0.4970	0.6722	-0.4669	-0.4663	-0.3131	-0.1695	1.0000	0.6930	0.7820	0.6198
Metastasis	-0.4808	0.8219	-0.5050	-0.3599	0.4513	0.6833	-0.3783	0.6646	0.7299	-0.4121	-0.5131	0.5867	-0.5475	-0.5546	-0.4752	-0.3777	0.6930	1.0000	0.8456	0.6615
pSMAD2	-0.4536	0.7431	-0.4597	-0.3148	0.6510	0.7040	-0.4556	0.6199	0.7388	-0.3597	-0.4968	0.6962	-0.5056	-0.5154	-0.4408	-0.2816	0.7820	0.8456	1.0000	0.7455
TGF-β 2	-0.7620	0.3687	-0.7246	-0.4455	0.7402	0.6785	-0.4840	0.6505	0.7013	-0.6948	-0.7525	0.7492	-0.8562	-0.8679	-0.5233	-0.5763	0.6198	0.6615	0.7455	1.0000

TRANSPARENT METHODS

Experimental model and research details

Mice and cell lines

Specific pathogen free, 6-8 weeks old female AKR/J mice were used for the study. Animals were purchased from the Jackson Laboratory and were maintained in pathogen free condition of central animal facility of the institute. All protocols involving animal experiments and human blood were approved by Institutional Ethics committee at the University of Burdwan. All animals were used according to the guidelines of the Institutional Dissection Monitoring Committee of The University of Burdwan. DL is a spontaneously developed murine lymphoma and was maintained in the peritoneum with periodic transfer of the tumor cells in female AKR/J mice (Hira et al., 2014b). Murine cell lines 2PK3, NIH/3T3 was purchased from National Cell Repository, NCCS, Pune India YAC1, CT26, Raji, THP-1, U937, and JE6.1 were purchased from ATCC, USA. DL, YAC1, Raji, THP-1, U937, JE6.1 and CT26 were maintained in RPMI-1640, while 2PK3 and NIH/3T3 were maintained in DMEM with 10% FBS.

Reagents and antibodies

Purified or PE, FITC, APC, or Alexa Fluor anti-mouse, CD3 (Cat# 100202, Biolegend), CD4 (Cat# 100416, 100408 Biolegend), CD8 (Cat# 100746, Biolegend), CD25 (Cat# 102014, 101907, Biolegend), FoxP3 (Cat# 32000, 126405, Biolegend), CD62L (Cat# 104402, Biolegend), CD44 (Cat# 103001, Biolegend), CD11b (Cat# 101207, Biolegend), CD11c (Cat# 117309, Biolegend), Class II(I-A/I-E) (Cat# 107605, Biolegend), CD86 (Cat# 105105, Biolegend), CD40 (Cat# 124601, Biolegend), CD80 (Cat# 104705, Biolegend), PD-1 (Cat# 135203, Biolegend) and isotype rat Abs were from Biolegend, USA. Purified anti-mouse CD16/32 (Cat# 101319, Biolegend) from Biolegend and TNF-α (Cat# 506331, Biolegend), TGF-β1, TGF-β1RI, TGF-β1RII, SMAD2/3, SMAD4, pSAMD2 from Cell signaling Technology, USA. Anti-mouse Neuropilin-1 was from R&D systems. Recombinant mouse TNF-α, IFN-γ, TGF-β1 from Invitrogen. Dynabeads™ Sheep-Anti Mouse IgG and HRP conjugated anti-rat secondary antibodies were purchased from Invitrogen. Unless otherwise stated, all other fine chemicals used in this study were obtained from Sigma-Aldrich, USA.

T cells and DC

CD3$^+$/CD4$^+$ or CD8$^+$T cells were isolated from single cell suspension of splenocytes or lymph nodes using negative selection criteria using Dynabeads (Invitrogen, USA) with recovery more than 96%. The purity of the cells was further checked by flow cytometry (>99%). Splenic CD11c$^+$ DC were enriched by negative selection before sorting. Following this procedure, CD11c$^+$ cells represented 30 ~ 40% of the cell suspension. CD11c$^+$ DC was further analyzed by flow cytometry into CD8$^+$ or CD8$^-$ CD11c$^+$ DC. Live cell numbers per culture were calculated from the yield by flow cytometry (Hira et al., 2014b; Hira et al., 2015b). Peripheral blood DCs from normal individual were isolated as described before (Hira et al., 2014b).

In vitro Studies: Drugs, growth inhibition and dose response IC$_{50}$ calculation

The TGF-βRI kinase inhibitor galunisertib (LY2157299 monohydrate), was obtained from Selleck Chemicals (S2230), Houston, TX. To evaluate the effect of galunisertib (DL, 2PK3, NIH/3T3) and recombinant TGF-β (DL, 2PK3, NIH/3T3, YAC1, CT-26) on cell proliferation, cells were plated in 96-well plates at 5×10^3 cells/well followed by treatment with increasing concentration of galunisertib (0, 0.025, 0.05, 0.10.25, 0.5, 1, 2.5, 5, 10µM) for 48 hours and rTGF-β (5ng/mL) for 96 hours & 168 hours. CellTiter 96® Non-Radioactive Cell Proliferation Assay (MTT) (Promega, Fitchburg, WI, USA) was used to quantify the cell proliferation according to the manufacturer's protocol(Hira et al., 2014a). IC$_{50}$ values of galunisertib were determined by curve fitting using non-linear regression (GraphPad Prism 8.0) which reports median-effect plots, the median dose (Dm, IC$_{50}$) and the correlation coefficient I. 95% confidence intervals of IC$_{50}$ was determined using GraphPad Prism 8 software.

DC functional assays: DC treatment with or without suboptimal dose of Galunisertib

Mouse CD11c$^+$ DC were cultured in 96-well plates with medium alone (DC) or in the presence of GM-CSF (1000 U/mL) (DC1), recombinant mouse IL-15 (200 pg/mL) (DC2) or LPS (5µg/mL) (DC3). After 6 hours, the cells were washed (×3), and the tumor cells were added, pretreated with or without 50 nM galunisertib to the wells at different E:T ratios depending upon the experimental protocol. In some experiments the DC were treated with a saturating concentration of antibodies to mouse TNF-α (50633, Biolegend) for 2 hours before the addition of tumor cells at an E:T ratio of 1:1. To assess the DC mediated growth inhibition (48 hours), cytotoxicity (18 hours) and apoptosis, MTT assay, LDH release assay and Annexin-FITC/PI staining was performed as describe earlier (Hira et al., 2014b).

Western blot

Cell lysates were analyzed by SDS-PAGE using the following antibodies: TGF-βRI (Rat mAb, MAB5871, R&D), TGF-βRII (Rabbit mAb, #79424, Cell Signaling Technology [CST]) (phospho-SMAD2(Ser465/467) (Rabbit mAb, #18338, CST), SMAD2/3 (Mouse mAb, #8685, CST), SMAD4 (Rabbit mAb #38454, CST), Mouse/Rat Neuropilin-1 (Goat Polyclonal, AF566, R&D). Secondary HRP-conjugated antibodies (Invitrogen) and enhanced chemiluminescence (GE Healthcare) was used to detect bound antibody. Whole and cytoplasmic protein levels were normalized to β-Actin expression (Mouse mAb #3700, CST) (Hira et al., 2015a).

In vivo studies: Tumor challenge and treatment experiments

DL tumor was maintained *in vitro* in RPMI 1640 (Invitrogen) supplemented with 10% FCS (Invitrogen) and in the peritoneum of AKR (H2k) mice as mentioned above. Female AKR/J mice (Jackson Laboratory) having weight 18-20 gm (n=12/group) were transplanted with DL tumor cells (3×10^4) and after 96 hours were treated with indicated concentrations of galunisertib. Tumor volume was calculated by measuring the abdominal circumference starting from day of tumor transplant. Control animals received vehicle only (2% DMSO+30% PEG 300+ddH$_2$O) by oral gavage once daily for the duration of the study. The treatment group received galunisertib at the rate of 10 mg, 50 mg & 75 mg per kg of body weight once daily in 2% DMSO+30% PEG 300+ddH$_2$O. Mice were under observation till day 60 when final data collection was made for Kaplan Meier survival analysis.

Adoptive transfer of CD11c$^+$ DC along with galunisertib

Mice (n=12/group) were transplanted with tumor and after 96 hours were treated with 6 intraperitoneal injections of rIL-15-activated DC (1×10^6 cells/mouse) either alone or in addition to galunisertib (10 mg/kg body weight) by oral gavage for 12 days. Altogether six galunisertib doses and six rIL-15 activated DC doses were given at an interval of 48 hours respectively. Mice were under observation for 80 days when final data collection was made for Kaplan Meier survival analysis.

Phenotypic and functional analysis of DC and T cells from tumor draining lymph nodes and spleen

Lymph node (LN) and spleen from five mice from each group (healthy control, DL tumor-bearing and vaccinated mice with galunisertib alone or in combination with rIL-15 activated DC) was selected for elective lymph node and spleen dissection. The study was performed following

institutional guidelines for the use of discarded tissue. Before surgery, blood sample was taken from each animal. Mouse myeloid DC (CD11c$^+$, MHC-II$^+$), T cells (CD4$^+$, CD8$^+$ and Treg) from normal, DL tumor-bearing or vaccinated groups were isolated as previously described. Parts of the LN & spleen were used for the histopathological analysis (Hira et al., 2015b).

CTL assay

CTL assays were performed as reported previously (Hira et al., 2015b). Briefly, effector CD8$^+$ T cells were isolated following negative selection using magnetic isolation kits from pooled splenocytes from various study groups and were incubated with target DL tumor cells at different effector-to-target ratios (1:1, 5:1, 10:1 & 25:1) for 8 hours. The lytic activity of CD8$^+$ T cells (% lysis) against DL cells was measured by an 18 hours non-radioactive cytotoxicity assay (Promega, USA).

Splenocytes stimulation studies

CD4$^+$ T cells from healthy control, DL tumor-bearing or surviving vaccinated mice were used as responder cells against the whole tumor lysate (10 μg/mL) pulsed and mitomycin C (10 μg/mL) treated stimulator DC, derived from the treated mice. The responder T cells (5×10^5) were co-cultured with stimulator DC (5×10^3) and the culture plates were incubated at 37°C, 5% CO$_2$ for 120 hours followed by MTT assay to determine the cell proliferation as describe previously (Hira et al., 2015b).

Flow cytometry

Freshly isolated LN or spleen cells were directly stained with conjugated antibodies and were analyzed by flow cytometry. For characterization of DC, mAbs recognizing CD11c, CD4, CD8, Class II, CD86, CD40 and CD83 (all from Biolegend) were used. Isolated CD4$^+$ T cells were first stained with anti-CD3, CD25, and Live/Dead stain with or without the other Abs and, after fixation, intracellular FOXP3 was stained. CD8$^+$ cells were stained with CD62L, CD44. CytoFLEX, Research Flow Cytometry were used for analysis (Beckman Coulter). The numbers of cells analyzed were 10,000 events per measurement and analyzed with FlowJo-10 software (Tree Star). For intracellular cytokine and Reactive oxygen species (ROS) estimations, the cells were stained with PE or FITC conjugated anti-mouse TNF-α, IFN-γ, TGF-β (Biolegend, USA), Neuropilin-1 (R&D) and CellRox Green (Invitrogen).

ELISA

Blood sample was collected from each treatment group including the non-immunized mice through the caudal vein and serum was separated on the indicated days. TNF-α, IFN-γ, TGF-β secretion was assessed by ELISA kit (Biolegend ELISA Max™) as per manufacturer's instruction and optical density at 450 nm was measured using microplate reader (Gupta et al., 2020).

Tissue processing and immunohistochemical analysis

Tissues (liver, lung, spleen and lymph node) were collected from healthy control, DL tumor-bearing and vaccinated mice and fixed in normal buffered formalin (NBF) and processed. Formalin-fixed, paraffin-embedded tissue sections were stained with Hematoxylin and Eosin (H&E) and were examined for regions of tumor metastasis. The immunohistochemical (IHC) procedure was performed on paraffin-embedded LN and spleen samples. IHC staining was performed using 5 µm tissue sections using Novolink Polymer Detection Systems (Leica, Germany) according to manufacturer's protocol. Briefly, after antigen retrieval with EDTA buffer (pH 8.0), samples were treated with anti-mouse primary antibodies (CD4, FOXP3, CD8, CD62L, CD44, pSMAD2) incubated overnight at 4°C. A secondary antibody was applied for 30 minutes at room temperature. Chromogenic detection of protein expression was determined in the presence of diaminobenzidine (DAB) and images were captured by Nikon 80i research microscope (400×).

Immunofluorescent staining

The staining of CD4, FOXP3 was carried out on serial paraffin sections of the spleen and CD3, CD8, PD-1 in TDLN. pSMAD2 staining was performed in cultured DL cells. DL cells cytosmear and cross-sections (5 µm) were incubated with the primary antibodies followed by the treatment with fluorescein conjugated antibody. For dual staining of CD4/FOXP3, CD3/CD8 or CD8/PD-1 the primary and secondary antibodies were used in sequences, based on optimum performance obtained in preliminary results. Slides were analyzed using Leica Dmi8 fluorescence microscope (Leica, Germany).

Statistical analysis

Unpaired, 2-tailed t test was used to compare pairs of groups, and Two-way ANOVA, Holm-Sidak Post-hoc test (*$p<0.05$, ** $p<0.01$, *** $p<0.001$) was performed for comparison in multiple group experiments using Prism 8 (GraphPad) software. Log-rank (Mantel-Cox) test was performed to define significant difference in survival between two groups in the therapeutic

studies. P values less than 0.05 were considered as significant. All values in the graphs are reported as mean ± SD. Multivariate analysis of mechanistic and survival data (e.g., LDA and PCA) was performed using JMP 15. Correlation study between FOXP3:CD4, CD62L:CD8 ratios were analyzed using the non-parametrical Spearman test.

Supplemental References

References

Gupta, U., Hira, S.K., Singh, R., Paladhi, A., Srivastava, P., and Pratim Manna, P. (2020). Essential role of TNF-α in gamma c cytokine aided crosstalk between dendritic cells and natural killer cells in experimental murine lymphoma. Int Immunopharmacol *78*, 106031.

Hira, S.K., Mishra, A.K., Ray, B., and Manna, P.P. (2014a). Targeted Delivery of Doxorubicin-Loaded Poly (ε-caprolactone)-b-Poly (N-vinylpyrrolidone) Micelles Enhances Antitumor Effect in Lymphoma. PLoS One *9*, e94309.

Hira, S.K., Mondal, I., Bhattacharya, D., Gupta, K.K., and Manna, P.P. (2015a). Downregulation of STAT3 phosphorylation enhances tumoricidal effect of IL-15-activated dendritic cell against doxorubicin-resistant lymphoma and leukemia via TNF-α. Int J Biochem Cell Biol *67*, 1-13.

Hira, S.K., Mondal, I., Bhattacharya, D., and Manna, P.P. (2014b). Downregulation of endogenous STAT3 augments tumoricidal activity of interleukin 15 activated dendritic cell against lymphoma and leukemia via TRAIL. Exp Cell Res *327*, 192-208.

Hira, S.K., Mondal, I., and Manna, P.P. (2015b). Combined immunotherapy with whole tumor lysate-pulsed interleukin-15-activated dendritic cells and cucurbitacin I promotes strong CD8(+) T-cell responses and cures highly aggressive lymphoma. Cytotherapy *17*, 647-664.